Hydraulics Research
Wallingford

THE DEVELOPMENT OF A NUMERICAL MODEL FOR THE SOLUTION OF THE BOUSSINESQ EQUATIONS FOR SHALLOW WATER WAVES

Constant depth case

J V Smallman BSc PhD
P F Matsoukis BSc PhD
A J Cooper MA PhD
E C Bowers BSc PhD DIC

Report No SR 137
August 1987

Registered Office: Hydraulics Research Limited,
Wallingford, Oxfordshire OX10 8BA.
Telephone: 0491 35381. Telex: 848552

This report describes work supported under contract PECD 7/6/053 funded by the Department of the Environment. The DOE nominated officer was Dr R Thorogood. Dr S W Huntington was Hydraulics Research's nominated officer. The report is published with the permission of the Department of the Environment but any opinions expressed are not necessarily those of the funding department.

The development of a numerical model for the solution of the Boussinesq equations for shallow water waves. Constant depth case. J V Smallman, P F Matsoukis, A J Cooper and E C Bowers. Report No SR 137, August 1987.

ABSTRACT

This report describes the development of a finite difference model to solve the Boussinesq equations in water of constant depth. The main objective of this work was to develop a mathematical model which can represent non-linear wave effects in harbours. In particular, it is important for the model to allow for an adequate description of the effects of set down beneath wave groups. This disturbance is known to be significant in assessing the movement of large moored vessels in harbours.

Prior to considering the finite difference model in detail some observations are made on the equations which represent the non-linear propagation of waves in shallow water. This is followed by a review of literature which describes work carried out by other researchers on solving the Boussinesq equation.

As a starting point for developing the mathematical model we first sought a solution to the one-dimensional form of the Boussinesq equations. Several finite difference schemes were considered, the one which was finally used was a predictor-corrector scheme implemented to take advantage of the computing power of the distributed array processor (DAP). The results from the model for the one dimensional case were compared with theoretical solutions and results from physical model tests. The mathematical model was found to give a good representative of non-linear wave propagation in one-dimension. In particular, within the limits of the Boussinesq equations, the numerical model was found to represent well the effects of set down beneath wave groups.

Having completed the solution to the one-dimensional equations the finite difference scheme was extended to the two dimensional case. Comparisons were again made between the model results and theoretical solutions, and the agreement was found to be good. The final series of tests done in the mathematical model were to provide a comparison with physical model results for the diffraction of set down. the comparison between the results demonstrated that the numerical model gave an accurate representation of diffraction of set down.

In conclusion, the mathematical model was found to provide an accurate numerical solution to the Boussinesq equations. In particular, it represented well the propagation of linear and non-linear waves in shallow water, taking into account both reflection and diffraction effects.

CONTENTS

CONTENTS (CONT/D)

FIGURES (CONT/D)

1 INTRODUCTION

Accurate predictions of wave conditions within a harbour are an important factor in optimising its layout. Until recently the only reliable method available to the engineer for estimating wave conditions in a harbour was to use a random wave physical model. However, advances made in mathematical modelling techniques in recent years have resulted in them becoming useful tools, both when used on their own at the early stages of design for a proposed harbour, and at the final design stage when used alongside a physical model. To date most of the mathematical models of wave action which have been developed are linear, and therefore will not represent non-linear effects as waves propagate in shallow water. One of the most important non-linearities in wave motion, as far as harbour response is concerned, is set down beneath wave groups. Obtaining an adequate description of the effects of set down is therefore an important factor which needs to be included in future mathematical models of waves in harbours.

This report describes the development of a two dimensional finite difference model to solve the Boussinesq equations. These equations represent the propagation of non-linear waves in shallow water, and have the property of providing an accurate description of set down beneath wave groups. A more detailed description of the Boussinesq equations and their properties is given in Chapter 2. In Chapter 3 we discuss the development and testing of a one-dimensional model of the Boussinesq equations, which provided an insight into the numerical methods, prior to solving the two-dimensional equations. The methods and results from the two-dimensional model are described in Chapter 4, and compared with results from other mathematical and physical models. In the final

chapter we give our conclusions and recommendations for future research.

2 BACKGROUND

2.1 Description of the general problem

Prior to discussing in more detail the Boussinesq equations, and their properties, it is worth making some observations in the equations which represent the non-linear propagation of waves in shallow water. Mathematically this process is described by the shallow water equations, which in two-dimensions are:

$$\frac{\partial z}{\partial t} + \frac{\partial}{\partial x}(uh) + \frac{\partial}{\partial y}(vh) = 0 \qquad (2.1)$$

$$\frac{\partial u}{\partial t} + u\frac{\partial u}{\partial x} + v\frac{\partial u}{\partial y} = -g\frac{\partial z}{\partial x} \qquad (2.2)$$

$$\frac{\partial v}{\partial t} + u\frac{\partial v}{\partial x} + v\frac{\partial v}{\partial y} = -g\frac{\partial z}{\partial y} \qquad (2.3)$$

where
z is elevation above datum, taken to be the still water level (m),
u,v, are depth averaged components of velocity in x,y direction respectively (m/s),
h is the total depth = d + z, d mean water depth (m) and
g is acceleration due to gravity (m/s^2).

In deriving equations (2.1) to (2.3) it is assumed that the fluid is homogeneous, isotropic and incompressible, and that all vertical acceleration, shear stress and Coriolis effects can be neglected. Equation (2.1) is then obtained by integrating the basic equation of conservation of mass, whilst (2.2)

and (2.3) are obtained from integrating the equation of conservation of momentum. A detailed derivation of equations (2.1) to (2.3) may be found in Stoker (Ref 1).

These equations are extensively used in river and tidal hydraulics where they provide an accurate description of fluid flow. However, the assumption made in their derivation that vertical accelerations can be neglected (ie that the flow is nearly horizontal) leads to the pressure within the fluid being hydrostatic. A direct consequence of this is that waves are propagated with a speed which is dependent, on water depth and current speed. This means that they are not dispersive, an assumption which is only realistic for very long waves.

Boussinesq (Ref 2) was the first to deviate from the assumption of negligible vertical acceleration by introducing a linear variation of the vertical velocity. This resulted in higher order terms being included in the equations, which represent the effects of small, but not negligible, vertical accelerations due to the curvature of the streamlines. The pressure is no longer hydrostatic and the waves retain their dispersive character i.e. their speed depends on both their wavelength and the water depth. For rather steep, non-linear waves this speed depends on wave height as well.

In recent years, Peregrine (Ref 3) extended Boussinesq's ideas to two spatial dimensions and also considered a gently varying sea bed. He presented the equations in the form in which they are now known:

$$\frac{\partial z}{\partial t} + \frac{\partial}{\partial x}(u\,h) + \frac{\partial}{\partial y}(v\,h) = 0 \qquad (2.4)$$

$$\frac{\partial u}{\partial t} + u\frac{\partial u}{\partial x} + v\frac{\partial u}{\partial z} = -g\frac{\partial z}{\partial x} + \frac{1}{2}d\left[\frac{\partial^3(u\,d)}{\partial x^2\,\partial t} + \frac{\partial^3(vd)}{\partial x\,\partial y.\,\partial t}\right]$$

$$-\frac{1}{6}d^2\left[\frac{\partial^3 u}{\partial x^2\,\partial t} + \frac{\partial^3 v}{\partial x\,\partial y\,\partial t}\right] \quad (2.5)$$

$$\frac{\partial v}{t} + u\frac{\partial v}{x} + v\frac{\partial v}{y} = -g\frac{\partial z}{\partial y} + \frac{1}{2}d\left(\frac{\partial^3(ud)}{\partial x\,\partial y\,\partial t} + \frac{\partial^3(vd)}{y^2\partial t}\right)$$

$$-\frac{1}{6}d^2\left(\frac{\partial^3 u}{\partial x\,\partial y\,\partial t} + \frac{\partial^3 v}{\partial y^2\,\partial t}\right) \quad (2.6)$$

Where the notation of (2.1) to (2.3) is preserved with $d \equiv d(x,y)$, ie the mean depth varies with x and y. Equation (2.4) is identical to (2.1) and represents conservation of mass, and (2.5) and (2.6) represent conservation of momentum.

Before discussing the dispersive properties of (2.4) to (2.6) it is worth observing that if the depth, d, is taken to be constant everywhere in the fluid domain then (2.4) to (2.6) become,

$$\frac{\partial z}{\partial t} + \frac{\partial}{\partial x}(uh) + \frac{\partial}{\partial y}(vh) = 0 \quad (2.7)$$

$$\frac{\partial u}{\partial t} + u\frac{\partial u}{\partial x} + v\frac{\partial u}{\partial y} = -g\frac{\partial z}{\partial x} + \frac{1}{3}d^2\left[\frac{\partial^3 u}{\partial x^2\partial t} + \frac{\partial^3 v}{\partial x\,\partial y\,\partial t}\right], \quad (2.9)$$

$$\frac{\partial v}{\partial t} + u\frac{\partial v}{\partial x} + v\frac{\partial v}{\partial y} = -g\frac{\partial z}{\partial y} + \frac{1}{3}d^2\left[\frac{\partial^3 u}{\partial x\,\partial y\,\partial t} + \frac{\partial^3 v}{\partial y^2\partial t}\right], \quad (2.9)$$

which is the form of the equation considered in this report.

The dispersive properties of the Boussinesq equations are most clearly illustrated by comparing the one-dimensional, linearised constant depth form of the equations,

$$\frac{\partial z}{\partial t} + d\,\frac{\partial u}{\partial x} = 0 \qquad (2.10)$$

and

$$\frac{\partial u}{\partial t} + g\frac{\partial z}{\partial x} = \frac{1}{3}\, d^2\, \frac{\partial^3 u}{\partial x^2 \partial t} \quad ; \qquad (2.11)$$

with the equation describing fluid motion in an incompressible, inviscid, irrotational fluid of constant depth, that is Laplace's equation,

$$\nabla^2 \phi = 0 \ ,$$

where ϕ is a velocity potential (see, for example, Stoker Ref 1). If we linearise the free surface boundary conditions then it can be shown that the dispersion relation is

$$\omega^2 = gk \tanh (kd),$$

where ω is the radian frequency, k is the wave number and g is the acceleration due to gravity. This can be approximated in polynomial form as

$$\omega^2 = gk\,(kd - 1/3\, d^3\, k^3 + \ldots) \qquad (2\ 12)$$

For shallow water, $kd \to 0$, the dispersion relationship above becomes $\omega^2 = gk^2 d$ and the phase velocity ω/k becomes $\sqrt{gd}$ which is independent of k, ie the waves are not dispersive.

The linearised version of the Boussinesq equations in the form (2.10) and (2.11) leads to a dispersion relation of the form

$$\omega^2 = \frac{gdk^2}{1 + 1/3\, k^2 d^2} \qquad (2.13)$$

which for small kd agrees with the expression (2.12) to the first two terms.

One of the basic properties of the Boussinesq equations is the possibility of transforming them to different forms by rewriting the third order term using the linearised shallow water equations. The term $\partial^3 u/\partial x^2 \partial t$ in (2.11) can be transformed to $\frac{\partial^3 z}{\partial x \partial t^2}$,

and the dispersion relation for small kd will remain the same as (2.13). However, it will be shown subsequently that the $\partial^3 u/\partial x^2 \partial t$ form of the third order term is preferable from the point of view of the numerical scheme. It is therefore equations (2.7) to (2.9) which are used in the present work. A more detailed discussion of the dispersive properties of the Boussinesq equations may be found in the Witham (Ref 4).

2.2 Review of recent literature

Research into methods of solving the Boussinesq equations numerically has in recent years been published predominantly by three groups of researchers. These are Abbott et al (see Refs 5 to 10), Hauguel (Ref 11) and more recently Schaper and Zeilke et al (Refs 12 to 15). The common element of all of the research published by these authors is that the governing equations are expressed in terms of volume flux densities p(=uh) and q(=vh) rather than in terms of vertically integrated velocities u and v, as in equations (2.4) to (2.6). In terms of p and q the Boussinesq equations become,

$$\frac{\partial z}{\partial t} + \frac{\partial p}{\partial x} + \frac{\partial q}{\partial y} = 0 \qquad (2.14)$$

$$\frac{\partial p}{\partial t} + \frac{\partial}{\partial x}\left(\frac{p^2}{h}\right) + \frac{\partial}{\partial y}\left(\frac{\partial q}{h}\right)$$

$$= -g\,\frac{h\partial z}{\partial x} + \tfrac{1}{2}dh\left[\frac{\partial^3}{\partial x^2\partial t}\left(\frac{dp}{h}\right) + \frac{\partial^3}{\partial x\,\partial y\,\partial t}\left(\frac{dq}{h}\right)\right]$$

$$- \frac{1}{6}d^2h\left[\frac{\partial^3}{\partial x^2\partial t}\left(\frac{p}{h}\right) + \frac{\partial^3}{\partial x\,\partial y\,\partial t}\left(\frac{q}{h}\right)\right] \qquad (2.15)$$

$$\frac{\partial q}{\partial t} + \frac{\partial}{\partial x}\left(\frac{pq}{h}\right) + \frac{\partial}{\partial y}\left(\frac{q^2}{h}\right)$$

$$= -gh\frac{\partial z}{\partial y} + \tfrac{1}{2}dh\left[\frac{\partial^3}{\partial y^2\partial t}\left(\frac{dq}{h}\right) + \frac{\partial^3}{\partial x\,\partial y\,\partial t}\left(\frac{dp}{h}\right)\right]$$

$$- \frac{1}{6}d^2h\left[\frac{\partial^3}{\partial x^2\partial t}\left(\frac{q}{h}\right) + \frac{\partial^3}{\partial x\,\partial y\,\partial t}\left(\frac{p}{h}\right)\right] \qquad (2.16)$$

where the notation of section (2.1) has been retained. The above equations are solved numerically using an implicit method by both Abbot et al (see Refs 6 and 9) and Schaper and Zeilke et al (see Refs 12 and 13). Hauguel (Ref 11) actually solves a more general form of the Boussinesq equations originally due to Serre (Ref 15). The Serre equations retain additional third order terms to those in the Boussinesq equations. In the derivation of (2.14) and (2.16) the convective part of the vertical acceleration term is neglected the bed variations are assumed to be gradual, and products of derivatives are assumed small in comparison to the derivatives themselves. If these simplifying assumptions are not made the more exact derivation results in the Serre rather than the Boussinesq equations. Mc Cowan (Ref 5) discusses the merits of retaining the extra 'Serre' terms and concludes that their contribution is insignificant compared to the main dispersive terms, and that the extra computational effort required to solve the Serre equations is not justified.

The starting point for most of the recent research was to demonstrate that the equations allowed both cnoidal and solitary wave profiles to propagate correctly ,see Abbott, Petersen and Skovgaard (Ref 7), and Schaper and Zeilke. (Ref 12). Cnoidal waves are permanent solutions of the Kortewag de Vries equations for waves moving in one direction (see Ref 4). As a consequence of this waves are also a permanent solution of the Boussinesq equations for uni-directional flow. A typical cnoidal wave is shown in Fig 1(a). One limiting case of the cnodial wave, in which the wavelength becomes infinite, corresponds to the solitary wave, see Fig 1(b).

Once authors had demonstrated that their method of numerical solution gave accurate results in one-dimension they then considered the two dimensional case. The problem most frequently treated in two dimensions was the refraction/diffraction of waves at a semi-infinite breakwater in water of constant depth. This has been covered in papers by Abbott et al (Ref 6), Hauguel (Ref 11) and Rottmann-Sode, Schaper and Zeilke (Ref 13).

In addition to presenting results from the numerical models, Abbott, Mc Cowan and Warren (Ref 9) also give a detailed analysis of the accuracy of their model, and describe the modifications to the finite difference schemes which are made to improve the accuracy of the results. A full discussion of the performance of this model and its range of application is given in Madsen and Warren (Ref 10). Aspects of the representation of open boundaries in the Abbott et al models are considered in Larsen and Dancy (Ref 8).

Finally, it should be observed that until recently there had been no work published on the use of the Boussinesq model in representing set down beneath wave

groups, a topic of major importance in the present work.

However, Prüser, Schaper and Zeilke have in the last few months presented a paper (Ref 14) which includes results modelling set down waves in a biochromatic wave system using the Boussinesq equations. Their results appear to be promising and indicate that the Boussinesq equations can represent the shoaling of set down with a reasonable degree of accuracy. The present report considers set down further in sections 3.3 and 4.3.

3 ONE-DIMENSIONAL EQUATIONS

3.1 Method of solution

3.1.1 Outline of approach

The one-dimensional form of the Boussinesq equations for the constant depth case is given by,

$$\frac{\partial z}{\partial t} + \frac{\partial}{\partial x}(uh) = 0 \qquad (3.1)$$

$$\frac{\partial u}{\partial t} + u\frac{\partial u}{\partial x} = -g\frac{\partial z}{\partial t} + \frac{1}{3}d^2\frac{\partial^3 u}{\partial x^2 \partial t} \qquad (3.2)$$

In seeking a numerical solution to these equations these are several different approaches which could be used. The one-dimensional form of the equations was therefore used to explore various methods of solution with a view to producing a numerical scheme which was stable, accurate and could take advantage of computing power of the distributed array processor (DAP) available at Hydraulics Research. All of the numerical schemes which were tested were based on the finite difference model for tidal flows (see Ref 15).

This model uses a second order accurate conditionally stable explicit scheme to solve the non-linear shallow water equations. The scheme is stable provided that the Courant number $Cr \leq 1$, where $Cr = (gd)^{\frac{1}{2}} \Delta t / \Delta x$. The finite difference equations are solved using a leap frog scheme on a mesh staggered in both space and time. In this section we consider an extension of this numerical scheme for the solution of the Boussinesq equations.

3.1.2 Linear terms

For the linearised one-dimensional shallow water equations the finite difference scheme can be expressed as

$$z^{n}_{i-\frac{1}{2}} = z^{n}_{i-\frac{1}{2}} - d\Delta t \frac{u^{n-\frac{1}{2}}_{i} - u^{n-\frac{1}{2}}_{i-1}}{\Delta x} \qquad (3.3)$$

$$u^{n+1/2}_{i} = u^{n-1/2}_{i} - g\,\Delta t \frac{z^{n}_{i+1/2} - z^{n}_{i-1/2}}{\Delta x} \qquad (3.4)$$

Where z is the elevation, u is the velocity in the x direction and Δx and Δt are the space and time increments. The notation $z^{n}_{i-\frac{1}{2}}$ refers to the finite

difference approximation to elevation at time $n\Delta t$ and position $(i-\frac{1}{2})\Delta x$, see figure 2. To extend (3.4) to include the third order dispersive term we require a finite difference approximation to $\frac{\partial^3 u}{\partial x^2 \partial t}$.

This approximation can simply be

$$\left[\frac{\partial^3 u}{\partial x^2 \partial t}\right]^{n} = \frac{u^{n+1/2}_{i+1} + u^{n+1/2}_{i-1} - 2u^{n+1/2}_{i+1} - u^{n-1/2}_{i+1}}{(\Delta x)^2 . \Delta t} - \frac{u^{n-\frac{1}{2}}_{i-1} + U^{n-\frac{1}{2}}_{i}}{} \qquad (3.5)$$

where the notation [ ] is used for finite difference approximation, the expression (3.5) arises from considering

$$\left[\frac{\partial^2 u}{\partial x^2}\right]^{n+\frac{1}{2}} = \frac{u_{i+1}^{n+\frac{1}{2}} - 2u_i^{n+\frac{1}{2}} + u_{i-1}^{n-\frac{1}{2}}}{(\Delta x)^2}$$

$$\left[\frac{\partial^2 u}{\partial x^2}\right]^{n-\frac{1}{2}} = \frac{u_{i+1}^{n-\frac{1}{2}} - 2u_i^{n-\frac{1}{2}} + u_{i-1}^{n-\frac{1}{2}}}{(\Delta x)^2}$$

The finite difference approximation (3.5) is second order accurate and its inclusion in (3.4) to represent the third order dispersion term leads to the following implicit numerical scheme.

$$z_{i-\frac{1}{2}}^{n} = z_{i-\frac{1}{2}}^{n-\frac{1}{2}} - \Delta t \frac{(u_i^{n-\frac{1}{2}} - u_{i-1}^{n-\frac{1}{2}})}{\Delta x} \qquad (3.6)$$

$$u_i^{n+\frac{1}{2}} = u_i^{n-\frac{1}{2}} - g\,\Delta t \frac{(z_{i+\frac{1}{2}}^{n} - z_{i-\frac{1}{2}}^{n})}{\Delta x}$$

$$+ \frac{d^2}{3} \frac{(u_{i+1}^{n+\frac{1}{2}} - 2u_i^{n+\frac{1}{2}} + u_{i-1}^{n+\frac{1}{2}} - u_{i+1}^{n-\frac{1}{2}} + 2u_i^{n-\frac{1}{2}} - u_{i-1}^{n-\frac{1}{2}})}{(\Delta x)^2}$$

It can be shown that the finite difference scheme represented in (3.6) is stable provided the Courant number, $Cr \leq 1$, where $Cr = (gd)^{\frac{1}{2}} \Delta t / \Delta x$.

Clearly, for the difference scheme to give an accurate solution to the differential equations it must display similar behaviour. In our discussion of the properties of Boussinesq equations in Section 2.1 it was shown that for the linearised form of the equations the dispersion relation is,

$$\omega^2 = \frac{gdk^2}{1+\frac{1}{3}k^2d^2} \qquad (3.7)$$

giving a phase velocity $\frac{\omega}{k} = (gd/(1+k^2d^2/3)^{\frac{1}{2}}$. From this expression it can be inferred that the third order terms act to reduce the shallow water phase velocity $(gd)^{\frac{1}{2}}$, and consequently the wavelength. It therefore needs to be demonstrated that the finite difference scheme also displays a reduction in wavelength on inclusion of the third order terms.

To examine this property further, the scheme given in (3.6) was implemented for the case of a channel of constant depth with a sinusoidal wave input. The total length of the channel was selected so that the wave front never reached its far boundary. This was done so that boundary conditions did not have to be applied, as these could have introduced numerical errors which would have contaminated the wave profile. The depth of the channel was taken to be 10m, and the input sine wave had an amplitude of 1.0m and a period of 10s. The wavelength of this wave corresponding to the shallow water speed $(gd)^{\frac{1}{2}}$ (= 9.91m/s) was 99.1m. The implicit numerical scheme was run using a space step Δx = 10m as this allowed sufficient points per wavelength to ensure that the wave was correctly resolved. (The number of points per wavelength is normally taken to be ≥ 8). The space step used was Δt = 1.0s, giving a Courant number of 0.99 which ensures that the scheme will be numerically stable.

In the numerical implementation of (3.4) the continuity equation remains explicit but the momentum equation takes the implicit form

$$e_i \; u_{i-1}^{n+1/2} + f_i \; u_i^{n+1/2} + g_i \; u_{i+1}^{n+1/2} = 0$$

for each velocity point i along the axis of the channel. The quantities e_i, f_i , and g_i, depend only on known values of the variables. Considering the total number of points, the above relationship leads

to a matrix equation of the form: $\underset{\sim}{A} \cdot \underset{\sim}{U} = \underset{\sim}{B}$ where $\underset{\sim}{U}$ is the matrix of the velocity values at each grid point and $\underset{\sim}{A}$ is a tridiagonal matrix. This equation is solved by means of a simple matrix inversion technique.

The results of running the model for this case with the implicit scheme are shown in Figure 3. It can be seen that the wave amplitude remains as before at 1.0m, but that the wavelength reduces by approximately 7% to a value of about 92m.

The same test was then repeated to test the performance of a numerical scheme of the predictor - corrector type. In this case the numerical solution is implemented in two parts. First, the finite difference equations are solved omitting the third order term. The values of the velocity u are used as a first approximation of the dispersive term (predictor stage). Then, using the calculated value of the 3rd order dispersive terms in the equation the values of z and u are updated (corrector stage). The corrector is then repeated as many times as are necessary to achieve convergence. For the simple one-dimensional test considered, it was not found necessary to iterate more than twice. The results (see Fig 4) are the same as before, i.e. the incident wave is propagated with a smaller phase velocity, and therefore, its wavelength is reduced. Theoretically, as the number of internal iterations tends to infinity, the solution should become identical to the one provided by the implicit scheme.

Within the context of linear dispersive equations, a qualitative test of the performance of our numerical scheme can be provided by running a solitary, instead of a sinusoidal wave at the model entrance and then monitoring its propagation along the channel. As has

been mentioned in Section 2.2, this sort of wave is a permanent solution of the Korteweg de Vries equation and consequently, of the Boussinesq equations for uni-directional flow. As such it will retain its shape undistorted as it propagates by balancing exactly non-linear with the dispersive effects. If the non-linear terms are excluded, the dispersive effects become absolutely dominant. As a result different parts of the wave start to travel with different speeds and the solitary wave breaks into a number of waves of different wave length. This type of propagation has an analytical solution (see Ref 4) but the purpose of the present experiment does not justify its practical implementation. The analytical solution shows that at the front, the wave tends to decay exponentially as time increases. In addition at the back of the wave a tail of short waves is formed which are moving with slower speeds, and that the further the wave lies from the front, the shorter its wavelength.

To test this case the scheme given in (3.4) was implemented for the constant depth channel situation described above, with an incident solitary wave of amplitude 1.0m. The results from the model are given in Figure 5 in the form of instantaneous wave profiles at different times as the solitary wave travels along the channel. It can be seen from Figure 5 that the numerical solution clearly displays all the features of the analytic solution described above.

3.1.3 Non-linear terms

Having considered the finite difference approximation of the dispersion term we now turn our attention to the non-linear terms in (3.2). In the first instance

the non-linear terms were represented using a similar method to that used in the Hydraulics Research tidal flow model (Ref 15). That is, the non-linear terms in (3.1) and (3.2) were represented by an explicit angled finite difference as scheme follows (see also Fig 2).

$$\left[\frac{\partial}{\partial x}(uh)\right] = \frac{u_i^{n-\frac{1}{2}}\,(d + J(z_{i-\frac{1}{2}}^{n-1})) - u_{i-1}^{n-\frac{1}{2}}\,(d + J(z_{i-3/2}^{n-1}))}{\Delta x}$$

where $J(z_{i-\frac{1}{2}}^{n-1}) = \frac{1}{2}\,(z_{i+\frac{1}{2}}^{n-1} + z_{i-\frac{1}{2}}^{n})$

for the continuity equation, and

$$\left[u\,\frac{\partial u}{\partial x}\right] = \bar{U}_o\,\frac{(J(u_{i+1}^{n+\frac{1}{2}}) - J(u_{i-1}^{n+\frac{1}{2}}))}{\Delta x}$$

where $\bar{U}_o = \frac{1}{2}\,(u_{i+1}^{n-\frac{1}{2}} + u_{i-1}^{n+\frac{1}{2}})$

and $J(u_{i+1}^{n+\frac{1}{2}}) = \frac{1}{2}\,(u_i^{n+\frac{1}{2}} + u_{i+1}^{n-\frac{1}{2}})$.

The finite difference approximation for the linear terms remains the same as described earlier this section.

So far we have demonstrated that the model is able to represent correctly the third order linear (dispersive) term. We now need to show that it can also model accurately the non-linear terms. For the non-linear equations there are few analytical solutions that can be used to check the results from the finite difference model. However, we can use the propagation of a solitary wave as a basic test, since if the finite difference model simulates accurately

both the dispersive and non-linear terms of the equations then, such a wave should retain its form unchanged as it travels along the channel. Because we have shown that the dispersive terms are modelled accurately, then if the solitary wave propagates undeformed we will have evidence that the non-linear terms are also being modelled correctly. For the solitary wave test we use the same flow, geometrical and operational details for the previous wave test were used. That is a channel depth of 10m, wave amplitude is 1.0m with Δx = 10m, Δt = 1s and Cr = 0.99. The results from this test are shown in Figure 6, from where it can be seen that the solitary wave does retain its shape while propagating along the channel. This shows that the numerical model simulates successfully all non-linear and dispersive effects in the one dimensional case.

Similar results are obtained, if we apply a predictor -corrector scheme. In this case, since we introduce an iterative procedure, there is no need to use angled approximations to the derivatives, and the finite difference scheme can be fully centered. The finite difference in predictor-corrector form for equations (3.1) and (3.2) which was used is as follows

$$z_{i-\frac{1}{2}}^{n} = z_{i-\frac{1}{2}}^{n-1} - \Delta t \frac{(u_i^{n-\frac{1}{2}} (Z_i^n + d) - u_{i-1}^{n-\frac{1}{2}} (Z_{i-1}^n + d))}{\Delta x} \tag{3.8}$$

where

$$Z_i^n = \frac{1}{4} (z_{i+\frac{1}{2}}^n + z_{i-\frac{1}{2}}^n + z_{i+\frac{1}{2}}^{n-1} + z_{i-\frac{1}{2}}^{n-1})$$

and

$$u_i^{n+\frac{1}{2}} = u_i^{n-\frac{1}{2}} - g\Delta t \frac{(z^n_{i+\frac{1}{2}} - z^n_{i-\frac{1}{2}})}{\Delta x}$$

$$- \Delta t \frac{(u_i^{n+\frac{1}{2}} + u_i^{n-\frac{1}{2}})}{2} \frac{(u_{i+1}^{n+\frac{1}{2}} - u_{i-1}^{n+\frac{1}{2}} + u_{i+1}^{n-\frac{1}{2}} - u_{i-1}^{n-\frac{1}{2}})}{4\Delta x}$$

$$+ \frac{d^2}{3} \left(\frac{u_{i+1}^{n+\frac{1}{2}} - 2u_i^{n+\frac{1}{2}} + u_{i-1}^{n+\frac{1}{2}} - u_{i+1}^{n-\frac{1}{2}} + 2u_i^{n-\frac{1}{2}} - u_{i-1}^{n-\frac{1}{2}}}{(\Delta x)^2} \right) \qquad (3.9)$$

The results for the predictor-corrector scheme using equations (3.8) and (3.9) for the case of a solitary wave in a channel of constant depth are shown in Figure 7. As for the implicit scheme it can be seen that the solitary wave retains its shape as it propagates along the channel.

Having examined the finite difference schemes for the linear case with sine waves and solitary waves as input, and the non-linear schemes with solitary waves as input it remains to examine the non-linear scheme with sine waves as input. The effects of introducing sine waves into a horizontal channel have been previously investigated both experimentally and numerically. Galvin (Ref 16) reports that when steep sinusoidal waves are generated in a horizontal channel the initial wave breaks down into a number of large and small waves. The smaller waves travel more slowly than the larger waves and therefore secondary crests develop behind the larger waves. These large waves are called solitons (waves resembling solitary waves) after an analogous phenomenon in plasma physics. There is, in general, interaction between these solitons, but if followed the separated waves will return, periodically in space, to approximate their sinusoidal, initial wave form. These results indicate that this initial sinusoidal wave form produced by the

wave generator can be thought of as the forced superposition of a number of solitary waves.

Madsen, Mei and Savage (Ref 17) have shown that these physical phenomena occur numerically by solving the appropriate equations using a characteristic based method. They demonstrated that some of the waves created resembled cnoidal waves rather than solitary waves and that, in general, the sort of waves produced depends on the value of the Ursell parameter Ur (Ur = a L^2/d^3).

Their experiments covered the range $2.5 < Ur < 500$ and their conclusions were

(a) For small values of Ur, the secondary crests take a long time to develop.

(b) For larger values of Ur, secondary crests appear sooner and in greater numbers, forming cnoidal waves at the front (for moderate Ur values, and solitary waves for large Ur values ($Ur > 60$).

(c) For $Ur > 100$, breaking starts to occur.

Since there is experimental and numerical evidence for such behaviour as described above, the finite difference model developed for the solution of the Boussinesq type equations should be able to demonstrate these basic features of non-linear wave propagation in shallow water. With this in mind, we examined, for a one-dimensional channel of depth 10.0m, the effects resulting from sinusoidal input waves with the following characteristics

- wave amplitude = 1.0m, wave period = 10 secs. ($Ur \simeq 10$)

- amplitude = 2.5m, wave period = 16 secs.
  (Ur ≃ 64)

The model was run using the predictor-corrector form of the scheme, the results are presented in Figures 8 and 9. It can be seen that they are in close agreement with the conclusions of Masden, Mei and Savage presented above. In the first case, (Fig 8) cnoidal waves are created at the front, while for the second case, (Fig 9) corresponding to large Ursell values, there are clearly solitary waves moving at the front of the wave train. This is confirmed also by comparing the numerical solution with the solitary wave profile provided by theory (see Fig 10).

This close agreement of the model results with experimental and theoretical evidence of non-linear wave propogation in shallow waters, shows that the finite difference scheme behaves in a satisfactory manner.

In addition, the same sort of test was repeated for an input wave representing the first two terms of the Stokes expansion of a cnoidal wave,

$$z = a \cos(\omega t - kx) + \frac{3\omega^2 a^2}{4g k^4 d^4} \cos 2(\omega t - kx) \qquad (3.10)$$

A cnoidal wave is a permanent wave solution of the Kortegweg de Vries equation and, thus, also of the Boussinesq type equations for uni-directional flow. If we were to apply as input conditions an infinite number of terms approximating the amplitude z of a cnoidal wave as above then the model should be able to retain the permanent wave form of this wave all along the channel, in similar way to the solitary wave. Since we are only using the first two terms of the

Stokes approximation and not a proper cnoidal wave, we do not expect to obtain exactly a permanent wave form.

The results from this test in the 10m constant depth channel are given in Fig 11. It can be seen that the cnoidal wave does not retain an exactly permanent form, but that the wave that is propagating is clearly close to cnoidal in shape. To achieve a true cnoidal profile an exact cnoidal form would need to be input to the model. In addition, by comparing Figure 11 with Figure 8, which was for a sine wave input, i.e. the first term of the cnoidal approximation, we can see that the effect of introducing the second order terms is to substantially improve the permanent wave form of propagating downstream.

3.1.4 Summary of approach

In summary, the one dimensional model tests described have been divided into two parts. First the linear equations were investigated using the finite difference scheme given by (3.6). These finite difference equations were implemented both as as implicit scheme and as a predictor-corrector scheme, and both of these were found to perform satisfactorily. Having examined the linear equations we turned our attention to the non-linear equations. Two finite difference schemes were tested to represent the non-linear terms: an explicit scheme with angled derivatives and an implicit scheme (implemented as a predictor-corrector scheme) with centred derivatives. Both of these schemes performed in a similar way. For both the linear and non-linear equations all the numerical tests were carried out using the $\frac{\partial^3 u}{\partial x^2 \partial t}$ version of the dispersion term. As discussed in

section 2.1 this version is equivalent to $\frac{\partial^3 z}{\partial x^2 \partial t}$ since for small kd they both lead to the same dispersion relation (2.13). The version $\frac{\partial^3 u}{\partial x^2 \partial t}$ has been used throughout the present work as it is in a more convenient form for the finite difference approach which is used here.

For subsequent development of the numerical model we need to select an appropriate form of the finite difference equations from those described in Sections 3.1.2 and 3.1.3. Because it was intended to implement the model on the Distributed Array Processor we require a scheme which is suitable for a parallel processing system. For the non-linear terms an explicit scheme with angled approximations to the partial derivatives cannot be easily implemented in a parallel processing system, whereas the fully centered finite difference scheme can. For these reasons the approach which was adopted for all the subsequent tests was to solve the Boussinesq equations with the finite difference scheme given by (3.8) and (3.9) using a predictor-corrector method on the DAP. The extension of (3.8) and (3.9) to the two dimensional case will be discussed in Chapter 4.

3.2 Boundary conditions

In all the one-dimensional tests described in 3.1 the mathematical model was set up so that waves did not reach the model boundaries. This situation is clearly artificial when waves are to be modelled in a harbour or at a coastal site. In these cases we require model boundaries which can represent beaches, armoured slopes or vertical walls, ie where the reflection behaviour of the structure can be taken

into account. As a first step we consider methods of modelling boundaries where the wave can pass through without any deformations which could cause reflections at these boundaries, and consequent numerical contamination of the solutions in the interior.

As a starting point we consider a wave entering a flume of finite length. We require boundary conditions at the opposite end of the flume to that at which the wave enters. This boundary is selected as a line of u velocity points. The velocity u at these points cannot be calculated using the basic finite difference scheme since no wave information is available at the outside of the boundary area. However, we can derive an expression for the u points at the boundary based on some assumptions about the approaching wave, and the reflection performance of the boundary based on the method of characteristics. For the linear form of the shallow water equations. The characteristics lines for the linear shallow water equations are given by

$$\frac{dx}{dt} = (gd)^{\frac{1}{2}}.$$

To derive appropriate boundary conditions for normally incident waves we need to consider the history of a wave travelling at a speed $(gd)^{\frac{1}{2}}$ arriving at a boundary point at time $(n+\frac{1}{2})\ \Delta t$. The characteristic line through a boundary point at time $(n+\frac{1}{2})\Delta t$ intersects the time level $(n-\frac{1}{2})\Delta t$ at a distance $(gd)^{\frac{1}{2}}\Delta t$ which is between $i\Delta x$ and $(i+1)\Delta x$, and which can be found by interpolation. It can be shown that the boundary condition has the form,

$$u_{i+1}^{n+\frac{1}{2}} = u_{i+1}^{n-\frac{1}{2}} - C_r\ (u_{i+1}^{n-\frac{1}{2}} - u_i^{n-\frac{1}{2}}), \qquad (3.11)$$

Where $Cr = (gd)^{\frac{1}{2}}\Delta t/\Delta x$ is the Courant number. Where

the Courant number is unity expression (3.11) becomes

$$u_{i+1}^{n+\frac{1}{2}} = u_i^{n-\frac{1}{2}}$$

and a wave should pass through the boundary unaltered. This situation is demonstrated for the present model in Figure 12 where a solitary wave is approaching an absorbing boundary, and the model parameters are such that Cr = 1. For the case where Cr ≠ 1 the solitary wave test was repeated, and it can be seen from Figure 13 that whilst the boundary condition performs relatively well there is some small numerical error involved. This error can be expected to increase as the numerical wave speed moves away from $(gd)^{\frac{1}{2}}$. It should also be observed that the derivation of the boundary condition (3.11) assumes waves to be normally incident at the boundary which will be true for the one-dimensional case, but will not hold in general. This point will be discussed further in section 4.2.

With these constraints in mind it was decided to explore other methods of representing absorbing boundaries in the mathematical model. One technique which has recently been reported by Larsen and Dancy (Ref 8) is that of using 'sponge layers' at the model boundaries. These layers typically consist of five to ten cells before the model boundary where the elevations and velocities are successively reduced prior to arriving at a condition of the form (3.10). The elevations and velocities are reduced in the sponge layer by division by a function $\mu(x)$ of the form,

$$\mu(x) = \exp\left[\left(2^{-(x_e-x)/\Delta x} - 2^{-(x_e-x_s)\Delta x)}\right)\log_e a\right], \quad (3.12)$$

Where $x = x_s$ is the start of the sponge layer and

$x = x_e$ is the end of the layer. It should be noted that at $x = x_s$, $\mu(x) = 1.0$, ie the wave enters the sponge layer undeformed, and that $\mu(x)$ is a monotonically increasing function of x. The parameter a is a constant which depends on the number of grid lines in the sponge layer. Typical values are a = 5 for a sponge layer 10 cells wide, and a = 2 for a sponge layer 5 cells wide.

A series of tests were done in the one dimensional model to examine the performance of the sponge layer, as given by (3.12). For all of these tests the model was set up to represent a wave flume 25m deep. In running the model a mesh size of 29m was used with a timestep of 1.18, giving a Courant number Cr = 0.64. For the first case which was considered a sine wave of period 14s and amplitude 1.61m was input at the open boundary. The resulting wave amplitudes at various locations along the flume were examined for runs of the model both without and with the sponge layer. In both cases the boundary condition applied at the end of the flume corresponds to (3.11). If the boundary conditions are working correctly we would expect the wave amplitude at the input frequency to stay constant at all positions along the flume. Any deviation from this constant value will be due to some wave energy being reflected from the boundary contaminating the solution in the interior (as demonstrated in Fig 13).

The results from the sine wave tests are summarized in Table 1, for the cases without a sponge layer, and with sponge layers 5 and 10 cells wide. It can be seen from table 1 that without the sponge layer the amplitudes along the flume varies between ±12% from the input amplitude of 1.61m. On introducing a sponge layer 5 cells wide the amplitudes at positions along the flume are within ±1% of the expected value.

Increasing the width of the sponge layer to 10 cells further improves the accuracy with the wave amplitudes having a value of 1.61m at all of the positions tested. Clearly as the width of the sponge layer increases its effectiveness also increases.

However, a balance needs to be achieved between the performance of the sponge layer and the amount of model space that it occupies. For the case described above the ten cell sponge layer will be approximately 1.4 wavelengths wide, and the five cell sponge layer 0.7 wavelengths wide. From their relative performances it appears that for optimum effectiveness the sponge layer needs to be of the order of one wavelength wide. For very long waves, this could lead to a large proportion of the model area being taken up by the sponge layer. This point will be particularly significant in the case of set down waves, and will be discussed further in section 3.3.

In addition to testing the sponge layer with a sine wave input, tests were also carried out using as input the first two terms of the Stokes expansion of a cnoidal wave, see expression (3.10). In this case we expect the wave amplitude to be constant at all positions along the flume at both the primary frequency (corresponding to T = 14s) and at the secondary frequency, provided the results are not contaminated by unwanted reflections from the absorbing boundary. The results from tests with these input conditions are summarised in Table 2. It can be seen that the sponge layer is again very effective for the primary wave frequency, as the amplitude remains constant along the flume. For the secondary wave frequency even with the sponge layer in place there is a variation in amplitude of about 12% from the expected value of 0.16m.

Finally, to illustrate that the cnoidal wave profile is propagating unchanged, and the sponge layer is effective reference should be made to Figure 14. This shows a plot of surface elevations at four different elapsed times. It can be seen that at all times the cnoidal wave profile is maintained throughout the length of the flume.

3.3 Set down wave tests

3.3.1 Background

All of the tests conducted so far have considered incident waves of only one frequency. We also need to know how the model responds to waves of several frequencies being propagated within its boundaries. Waves propagate at speeds which depend on their period and therefore, they will continually move through each other. At certain times a number of them will come together to produce a group of large waves while at other times they will be out of phase giving rise to relatively small waves. When a group of large waves is formed, there is a corresponding increase in the kinetic energy of orbital water particle movement. This leads to a reduction in the water pressure and if the air pressure is taken to be constant, the result is that a depression in the mean water level occurs beneath groups of high waves. A compensating rise in the mean level occurs between groups of high waves. This surface perturbation is enhanced by a wave-like flow that develops beneath the surface. This disturbance is known as set down beneath wave groups and was first described by Longuet-Higgins (Ref 18). It has a periodicity associated with the groups but it differs from a free long wave, because it is tied to the wave group. Therefore it propagates at the group velocity, which is less than the phase velocity of a free long wave of the same period as the set down.

This disturbance with period of the order of minutes is extremely important for large moored vessels, since the natural periods of horizontal oscillation of such vessels on their moorings are typically within the range of 30 sec to 2 minutes. As a result, a significant resonant response of the vessel can be produced by relatively small amplitude long period wave motions, which in certain cases can cause moorings to part. The problem can be compounded for vessels moored inside harbours when long period wave motions are amplified through harbour resonance, since it has been shown by Bowers (Ref 19) that set down behaves much like an ordinary long wave when it excites the resonant modes of harbours.

The simplest example of set down beneath wave groups is provided by a system consisting of sine waves at two frequencies, the groups of waves (and hence the set down) occur regularly with a frequency equal to the difference between the two primary frequencies. Physical model tests using regular wave groups and random seas have been carried out by Bowers (Ref 20). It was found during these tests that the wave generator had to be programmed to produce the correct representation of set down beneath wave groups. The effect of not programming the wave generator to produce set down is to introduce spurious long waves with the same period and a phase shift of 180° so that the boundary condition on the paddle face, $u_x^{(2)} = 0$, is satisfied. As the primary wave system propagates away from the generator, it carries with it the set down associated with wave groups but, also, propagating with the system are the spurious long waves. As has been mentioned above, set down propagates more slowly than the free secondary long waves. They are exactly out of phase at the wave generator and will gradually come into phase with one

another with increasing distance from the generator. As the distance increases further the two will again go out of phase and so on. Thus, the response of harbour and moored ships sensitive to long period disturbances could depend on their distance from the wave maker.

Similar reasoning to this also applies to numerical models. That is, care must be taken when specifying the input boundary conditions to the numerical model to ensure that set down is correctly represented.

For the Boussinesq model the main characteristics of the set down wave can be predicted by examining the differential equations (3.1) and (3.2). By expanding the various terms in these equations to second order it can be shown that the profile of the set down wave is,

$$D \cos (\omega_- t - k_- x)$$

where $\omega_- = \omega_2 - \omega_1$

$$k_- = k_2 - k_1$$

and ω_1, ω_2 and k_1, k_2 are the angular frequencies and wave numbers of th two primary waves. The amplitude of the set down wave is given by,

$$D = \frac{a_1 a_2}{2d} \frac{k_-}{\omega_-} \left(k_- d \, \frac{\left(\frac{\omega_-}{d} \frac{\omega_1}{k_1} \frac{\omega_2}{k_2} + g k_- \left(\frac{\omega_1}{k_1} + \frac{\omega_2}{k_2}\right)\right)}{\omega_-^2 \left(1 + \frac{k_-^2 d^2}{3}\right) - g d k_-^2} + \left(\frac{\omega_1}{k_1} + \frac{\omega_2}{k_2}\right)\right) \tag{3.13}$$

where a_1 and a_2 are the primary wave amplitudes.

The expression (3.13) for the set down amplitude derived from the Boussinesq equations differs from that which is derived using Laplaces equation and free surface boundary conditions taken to second order. The expression for the amplitude of set down in this case is,

$$D = \frac{1}{g}\left(\omega_- A \cosh k_- d + \frac{a_1 a_2 g}{2}\left(k_1 \tanh k_1 d + k_2 \tanh k_2 d\right)\right.$$
$$\left. - g^2 \frac{k_1 k_2 a_1 a_2}{2\omega_1 \omega_2} \quad \frac{\cosh k_+ d}{\cosh k_1 d \cosh k_2 d}\right)$$

where

$$A = a_1 a_2 g^2 \left(\frac{2k_1 k_2 \omega_-}{\omega_1 \omega_2}(1 + \tanh k_1 d \tanh k_2 d) + \frac{k_2^2}{\omega_2 \cosh^2 k_2 d}\right.$$
$$\left. - \frac{k_1^2}{\omega_1 \cosh^2 k_1 d}\right) / 2(\omega_-^2 \cosh k_- d - g k_- \sinh k_- d) \quad (3.14)$$

Clearly, the expression (3.13) and (3.14) cannot be expected to be the same as they arise from two different equations. However, because the dispersion relation from the Boussinesq equation is a reasonable approximation to the more exact dispersion relation obtained using potential theory, we can expect the set down amplitude given by (3.13) to be a reasonable approximation to that given by (3.14). The approximation given by (13.3) improves as the water depth decreases. An indication of the discrepancy between the values of the two expressions for specific cases will be given in the subsequent section.

3.3.2 Discussion of results from set down wave tests

A series of tests were carried out using regular wave groups with the numerical model set up to represent a wave flume of constant depth. For the one dimensional case two particular features were examined in these tests. The first was that the model represented correctly set down beneath regular wave groups, and the second was to see how well the sponge layer boundary conditions performed with waves of lengths corresponding to the set down frequency. A consequence of both of these objectives was that some tests were also needed to investigate the number of grid points per wavelength which are required to achieve a good representation of both the primary and set down wave effects.

The first set of tests which were done were with the numerical model representing a flume of depth 25m, and for incident waves for a regular wave group with the following characteristics.

	Frequency (Hz)	Amplitude (m)	Wavelength (m)
Primary wave one	0.10	1.97	128
Primary wave two	0.07	1.65	202
Set-down	0.03	0.23	513*

(* Actually the wavelength of a free wave at the set down frequency).

The amplitude of the set down was calculated using expression (3.13). If this group of waves is propagating correctly in a flume of constant depth then the amplitude of each of the frequency components should remain constant throughout the length of the flume. Therefore, during runs of the model time

series of surface elevations were collected at a number of positions along the flume, and a spectral analysis performed to obtain the amplitudes of each of the frequency components at these positions. The model was first run with a boundary condition of the form (3.11), with a mesh size Δx = 15m. This mesh size gives approximately 8.5 points for the shortest primary wavelength. The time step was selected to be Δt = 0.66s, giving a Courant number of 0.69 which satisfies the stability constraint for this scheme. Two further runs of the model were also made using sponge layer boundary conditions with sponge layer widths of 10 cells and 20 cells. The results from these tests are summarised in Table 3.

It can be seen from Table 3 that for the model run without the sponge layer the wave amplitude at all three frequencies varies greatly about the expected value. For the cases with the sponge layers in place the results with the 10 and 20 cell layers are very similar. With the sponge layer boundary conditions the variation in the primary wave amplitude is much smaller than in the case without the sponge layers, all of the values being within 10% of the expected value. However, both without and with the sponge layers there is still a significant variation in the amplitude of the set down wave, although this variation is slightly less where the sponge layer boundary condition was used.

As discussed previously there are two possible causes for the set down amplitude to vary in this way, either there are unwanted reflections from the boundaries entering the model area or the model representation could be improved. The first cause has been explored, to some extent, in the tests described above. The second was investigated by decreasing the grid size in the model to Δx = 12.5m, this gave approximately 10

points for the shortest primary wavelength, which should improve the accuracy of the model. For this case the time step was selected to be $\Delta t = 0.55s$, giving a Courant number of 0.69. For these parameters the model was again run without a sponge layer, and with sponge layers of 10 and 20 cells width. The results from these tests are summarised in Table 4.

It can be seen from Table 4 that without the sponge layer there is, as in Table 3, significant variation in the amplitudes of waves at all three frequencies. Introduction of the sponge layer improves the accuracy of the primary waves, and for the finer mesh these are closer to their expected value than for the more coarse mesh. The values of the set down wave amplitude with the sponge layer boundary conditions are now fairly close to their expected value. Consideration was given to reducing the mesh size again to see if the accuracy of the set down amplitudes would be improved further. However, numerical experiments demonstrated that the mesh size used must be greater than half the depth for the model to remain stable. Therefore for a depth of 25m the minimum mesh size which could be used was $\Delta x = 12.5m$, which had already been tested.

To examine further the accuracy of representation of regular wave groups in the numerical model a second series of tests were done with the model set up to represent a flume of 10m depth. The characteristics of the incident waves were,

	Frequency (Hz)	Amplitude (m)	Wavelength (m)
Primary wave one	0.10	0.5	92
Primary wave two	0.07	0.3	137
Set down	0.03	0.075	328*

(* Actually the wavelength of a free wave at the set down frequency).

The model was run using a boundary condition with a sponge layer 10 cells wide. The first run was for a mesh size Δx = 15m, giving approximately 6 points to the shortest primary wavelength. The time step was chosen to be Δt = 0.96s giving a Courant number of 0.64. The results from this run for the set-down and primary waves are given in Table 5.

It can be seen from Table 5 that for the 15m mesh case there is substantial variation in the expected wave amplitudes for both the primary and the set down waves. The same test was repeated using a 5m mesh with a time step of 0.35s, giving a Courant number of 0.64. Using Δx = 5m gives 18 points to the shortest primary wavelength. The results from this test are also given in Table 5. It can be seen that for the 5m mesh case the amplitudes at all frequencies are within 10% of their expected value. These results appear to confirm that in order to correctly represent secondary effects, such as the set down, which result from the non-linear interaction of primary waves, the primary wave components must be modelled as accurately as possible.

Finally, a comparison is given between the results of a physical model test using regular wave groups, and those from the numerical model, using two different mesh sizes, as given in Tables 3 and 4. The comparison of the amplitudes at the set down frequency is given in Table 6. It should be noted that the set down amplitude in the numerical model is expected to be 0.23m (equation 3.13), whereas for second order potential theory it is expected to be 0.28m (equation 3.14). In the physical model measurements of the set down amplitude were made at positions 3L/2, 7L/4

....., where L is the wavelength of the free wave at the set down frequency. These locations were selected because as they are at distances from the paddle at which the effects of the reflection of set down from the shingle beach at the end of the wave flume will be minimised. The reasons for this are discussed in Reference 20. Reflections from the shingle beach are probably the cause of the small variations in physical model set down amplitudes shown in table 6. Although at all these points the measured set down amplitude varies by less than 4% from the value predicted by second order potential theory. The set down amplitude predicted by the Boussinesq equations (0.23m) is 18% less than the potential theory value, which reflects the approximate nature of the Boussinesq equations.

It can be seen from table 6 that for the 12.5m mesh case the Boussinesq model results are with 10% of the expected value of 0.23. The exceptions to this are at 13L/4 and 7L/4 where the numerical model result is about 20% less than the expected value. These variations are probably not due to reflections of the sort described above for the physical model. It is more likely that they are due to numerical error, and that they could be decreased by using a finer mesh. Evidence of this can be seen in table 5.

The approximate nature of the set down representation in the Boussinesq model is also illustrated in the case shown in table 5. For 10m depth, where we expect the shallow water approximations to provide a better approximation, the set down amplitude of 0.075m expected from the Boussinesq equations (3.13) is 7% lower than the 0.081m value predicted by second order potential theory (3.14). This demonstrates that, whilst the Boussinesq equations only approximate the value of set down amplitude predicted by second order

potential theory, this approximation becomes better in as the water depth decreases.

From the results described in this section we can conclude that, within the limits of the Boussinesq approximation, the numerical model represents well set down effects provided a sufficiently fine mesh is used.

4 TWO DIMENSIONAL EQUATIONS

4.1 Method of solution

The two dimensional form of the Boussinesq equations for the constant depth case are,

$$\frac{\partial z}{\partial t} + \frac{\partial}{\partial x}(uh) + \frac{\partial}{\partial y}(vh) = 0 \qquad (4.1)$$

$$\frac{\partial u}{\partial t} + u\frac{\partial u}{\partial x} + v\frac{\partial u}{\partial y} = -g\frac{\partial z}{\partial x} + \frac{1}{3}d^2\left(\frac{\partial^3 u}{\partial x^2 \partial t} + \frac{\partial^3 v}{\partial x \partial y \partial t}\right) \qquad (4.2)$$

$$\frac{\partial v}{\partial t} + u\frac{\partial v}{\partial x} + v\frac{\partial v}{\partial y} = -g\frac{\partial z}{\partial y} + \frac{1}{3}d^2\left(\frac{\partial^3 u}{\partial x \partial y \partial t} + \frac{\partial^3 v}{\partial y^2 \partial t}\right) \qquad (4.3)$$

The method of solution of these equations is derived from the method finally chosen for solving the one-dimensional equations which was discussed in the previous chapter. The finite difference scheme which was used to solve (4.1) to (4.3) is as follows:

$$z^{n}_{i-\frac{1}{2},j-\frac{1}{2}} = z^{n-1}_{i-\frac{1}{2},j-\frac{1}{2}} - \Delta t\,\frac{\left(u^{n-\frac{1}{2}}_{i,j-\frac{1}{2}}\,(Zx^{n}_{i,j-\frac{1}{2}}+d) - u^{n-\frac{1}{2}}_{i-1,j-\frac{1}{2}}(Zx^{n}_{i-1,j-\frac{1}{2}}+d)\right)}{\Delta x}$$

$$-\Delta t\frac{\left(v^{n-\frac{1}{2}}_{i-\frac{1}{2},j}\,(Zy^{n}_{i-\frac{1}{2},j}+d) - v^{n-\frac{1}{2}}_{i-\frac{1}{2},j-1}(Zy^{n}_{i-\frac{1}{2},j-1}+d)\right)}{\Delta y} \qquad (4.4)$$

where $Zx^{n}_{i,j-\frac{1}{2}} = \frac{1}{4}(z^{n}_{i+\frac{1}{2},j-\frac{1}{2}} + z^{n}_{i-\frac{1}{2},j-\frac{1}{2}} + z^{n-1}_{i+\frac{1}{2},j-\frac{1}{2}} + z^{n-1}_{i-\frac{1}{2},j-\frac{1}{2}})$,

and $Zy^{n}_{i-\frac{1}{2},j} = (z^{n}_{i-\frac{1}{2},j+\frac{1}{2}} + z^{n}_{i-\frac{1}{2}j-\frac{1}{2}} + z^{n-1}_{i-\frac{1}{2},j+\frac{1}{2}} + z^{n-1}_{i-\frac{1}{2},j-\frac{1}{2}})$

$$u^{n+\frac{1}{2}}_{i,j-\frac{1}{2}} = u^{n-\frac{1}{2}}_{i,j-\frac{1}{2}} - g\Delta t\,\frac{(z^{n}_{i+\frac{1}{2},j-\frac{1}{2}} - z^{n}_{i-\frac{1}{2},j-\frac{1}{2}})}{\Delta x}$$

$$- \Delta t\,\frac{(u^{n+\frac{1}{2}}_{i,j-\frac{1}{2}} + u^{n-\frac{1}{2}}_{i,j-\frac{1}{2}})}{2}\,\frac{(u^{n+\frac{1}{2}}_{i+1,j-\frac{1}{2}} - u^{n+\frac{1}{2}}_{i-1,j-\frac{1}{2}} + u^{n-\frac{1}{2}}_{i+1,j-\frac{1}{2}} - u^{n-\frac{1}{2}}_{i-1,j-\frac{1}{2}})}{4\Delta x}$$

$$-\Delta t\; V^{n}_{i,j-\frac{1}{2}}\,\frac{(u^{n+\frac{1}{2}}_{i,j+\frac{1}{2}} - u^{n+\frac{1}{2}}_{i,j-3/2} + u^{n-\frac{1}{2}}_{i,j+\frac{1}{2}} - u^{n-\frac{1}{2}}_{i,j-3/2})}{4\Delta y}$$

$$+\frac{d^2}{3}\,\frac{(u^{n+\frac{1}{2}}_{i+1,j-\frac{1}{2}} - 2u^{n+\frac{1}{2}}_{i,j-\frac{1}{2}} + u^{n+\frac{1}{2}}_{i-1,j-\frac{1}{2}} - u^{n-\frac{1}{2}}_{i+1,j-\frac{1}{2}} + 2\,u^{n-\frac{1}{2}}_{i,j-\frac{1}{2}} - u^{n-\frac{1}{2}}_{i-1,j-\frac{1}{2}})}{(\Delta x)^2}$$

$$+\frac{d^2}{3}\,\frac{(v^{n+\frac{1}{2}}_{i+\frac{1}{2},j} - v^{n+\frac{1}{2}}_{i-\frac{1}{2},j} - v^{n+\frac{1}{2}}_{i+\frac{1}{2},j-1} + v^{n+\frac{1}{2}}_{i-\frac{1}{2},j-1} - v^{n-\frac{1}{2}}_{i+\frac{1}{2},j} + v^{n-\frac{1}{2}}_{i-\frac{1}{2},j} + v^{n-\frac{1}{2}}_{i+\frac{1}{2},j-1} - v^{n-\frac{1}{2}}_{i-\frac{1}{2},j-1})}{\Delta x\;\Delta y} \tag{4.5}$$

where

$$V^{n}_{i,j-\frac{1}{2}} = \frac{1}{8}(v^{n+\frac{1}{2}}_{i+\frac{1}{2},j} + v^{n+\frac{1}{2}}_{i-\frac{1}{2},j} + v^{n+\frac{1}{2}}_{i-\frac{1}{2},j-1} + v^{n+\frac{1}{2}}_{i-\frac{1}{2},j-1} + v^{n-\frac{1}{2}}_{i+\frac{1}{2},j} + v^{n-\frac{1}{2}}_{i-\frac{1}{2},j} + v^{n-\frac{1}{2}}_{i+\frac{1}{2},j-1} + v^{n-\frac{1}{2}}_{i-\frac{1}{2},j-1})$$

$$v^{n+\frac{1}{2}}_{i-\frac{1}{2},j-1} = v^{n-\frac{1}{2}}_{i-\frac{1}{2},j-1} - g\Delta t\,\frac{(z^{n}_{i-\frac{1}{2},j-\frac{1}{2}} - z^{n}_{i-\frac{1}{2},j-3/2})}{\Delta t}$$

$$- \Delta t\; U^{n}_{i-\frac{1}{2},j-1}\,\frac{(v^{n+\frac{1}{2}}_{i+\frac{1}{2},j-1} - v^{n+\frac{1}{2}}_{i-3/2,j-1} + v^{n-\frac{1}{2}}_{i+\frac{1}{2},j-1} - v^{n-\frac{1}{2}}_{i-3/2},j-1)}{4\Delta y}$$

$$-\Delta t\,\frac{(v^{n+\frac{1}{2}}_{i-\frac{1}{2},j-1} + v^{n-\frac{1}{2}}_{i-\frac{1}{2},j-1})}{2}\,\frac{(v^{n+\frac{1}{2}}_{i-\frac{1}{2},j} - v^{n+\frac{1}{2}}_{i-\frac{1}{2},j-2} + v^{n-\frac{1}{2}}_{i-\frac{1}{2},j} - v^{n-\frac{1}{2}}_{i-\frac{1}{2},j-2})}{4\Delta y}$$

$$+\frac{d^2}{3}\,\frac{(u^{n+\frac{1}{2}}_{i,j-\frac{1}{2}} - u^{n+\frac{1}{2}}_{i-1,j-\frac{1}{2}} - u^{n+\frac{1}{2}}_{i,j-3/2} + u^{n+\frac{1}{2}}_{i-1,j-3/2} - u^{n-\frac{1}{2}}_{i,j-\frac{1}{2}} + u^{n-\frac{1}{2}}_{i-1,j-\frac{1}{2}} + u^{n-\frac{1}{2}}_{i,j-3/2} - u^{n-\frac{1}{2}}_{i-1,j-3/2})}{\Delta x\;\Delta y}$$

+ .....

$$\pm\frac{d^2}{3}\frac{(v^{n+\frac{1}{2}}_{i-\frac{1}{2},j}-2v^{n+\frac{1}{2}}_{i-\frac{1}{2},j-1}+v^{n+\frac{1}{2}}_{i-\frac{1}{2},j-2}-v^{n-\frac{1}{2}}_{i-\frac{1}{2},j}+2v^{n-\frac{1}{2}}_{i-\frac{1}{2},j-1}-v^{n-\frac{1}{2}}_{i-\frac{1}{2},j-2})}{(\Delta y)^2} \tag{4.6}$$

where

$$U^n_{i-\frac{1}{2},j-1} =$$

$$\frac{1}{8}(u^{n+\frac{1}{2}}_{i,j-\frac{1}{2}}+u^{n+\frac{1}{2}}_{i-1,j-\frac{1}{2}}+u^{n+\frac{1}{2}}_{i,j-3/2}+u^{n+\frac{1}{2}}_{i-1,j-3/2}+u^{n-\frac{1}{2}}_{i,j}+u^{n-\frac{1}{2}}_{i-1,j-3/2}+u^{n-\frac{1}{2}}_{i,j-3/2}+u^{n-\frac{1}{2}}_{i-1,j-3/2})$$

The finite difference scheme given by (4.4) to (4.6) is implemented as a predictor-corrector scheme. First, the finite difference equations are solved omitting the dispersive terms, (predictor stage). The calculated values of u and v are used to make a first approximation to the dispersive terms which are then used in the equations to update the values of z,u and v (corrector stage). The corrector is then repeated until convergence is achieved (in practice this involves about six iterations of the corrector). It can be shown that the finite difference scheme represented by (4.4) to (4.6) is stable provided $Cr \leqslant 1/\sqrt{2}$.

As with the one-dimensional case the problem arises of verifying that the numerical model is producing accurate solutions, given the lack of analytical solutions against which to compare it. As a starting point we again consider the solitary wave, which should retain its initial shape as it propagates in water of constant depth provided that the non-linear terms in (4.1) to (4.3) are exactly balanced against the dispersive terms.

To illustrate that the model can propagate a solitary wave correctly we consider a long crested solitary wave entering a square basin with its crest at 45° to the basin sides (see Fig 16). In this case the depth of the basin is taken to be 10m and the wave amplitude 1.0m. A time increment Δt = 1s was used with a mesh size Δx of 14m, giving a Courant number of 0.707 which satisfies the stability criterion. The model was run for a large number of time steps, but care was taken to ensure that the wave did not reach the end limits of the basin area, so that boundary conditions did not have to be applied there. The propagation of the wave inside the basin was monitored and the results presented in the form of surface elevations in a cross-section along the diagonal at various time levels (Fig 16). By comparing the shape of the wave at these times and with the theoretical profile, we can conclude that this shape remains unchanged during the wave propagation. This provides evidence that the finite difference model does simulate accurately the non-linear and dispersive terms of the equations and therefore can be considered as a reliable means for the numerical integration of the Boussinesq equations in two spatial dimensions. The same test was repeated for a 30° incidence angle. The cross-sections at various time levels are now taken not along the diagonal of the basin but along the line at 30° to the horizontal x-axis. The results (Fig 17) verify that the numerical model retains not only the shape of the solitary wave but, also its angle of propagation in the interior of the basin area.

In both of the tests described above, waves were not allowed to reach the model boundary. We now need to consider situations where waves impinge on the boundaries, and how to represent boundary conditions there.

4.2 Boundary conditions

The first type of boundary condition to be considered is one where the wave can pass through the boundary without deformations. Initially, we return to a boundary condition of the form (3.11) which is based on the characteristic lines of the linearised shallow water equations. As an example of this type of boundary condition we consider the situation where the wave approaches the boundary at 45°. In this case the characteristic lines will be defined by $\frac{dx}{dt} = (gd)^{\frac{1}{2}} \cos 45°$ and $\frac{dy}{dt} = (gd)^{\frac{1}{2}} \sin 45°$, and we can show that the boundary condition is,

$$u_{i+1}^{n+\frac{1}{2}} = u_{i+1}^{n-\frac{1}{2}} - \frac{Cr}{\sqrt{2}} (u_{i+1}^{n-\frac{1}{2}} - u_{i}^{n-\frac{1}{2}}), \qquad (4.7)$$

where Cr is the Courant number. Where the Courant number is exactly $1/\sqrt{2}$ the boundary condition (4.7) becomes,

$$u_{i+1}^{n+\frac{1}{2}} = (\frac{g}{2d})^{\frac{1}{2}} z_{i+\frac{1}{2}}^{n},$$

and a wave at 45° should pass through the boundary undistorted.

To test this boundary condition we consider the case described in the previous section of a solitary wave entering a square basin at an angle of 45°. The surface elevation contours at the boundary for this case are shown in Figure 18. It can be seen that the solitary wave leaves the model area without any deformation or reflections from the boundary. The formulation of the boundary conditions described above assumes a prior knowledge of the angle of incidence of a wave at an end boundary. This is not, in general,

the case and therefore we have to assess the effect of using in the absorbing boundary conditions an angle which is different from the angle of incidence.

We consider solitary waves entering the square basin at an angle of 60°, while we retain the form of boundary conditions described above for an angle of 45°. We present the results as contour lines of surface elevation (Fig 19). There is a certain deformation of the wave at its crest close to the end boundary and in general, the contours do not remain absolutely straight. Numerical errors start to propagate from the absorbing boundary in to the area inside the model. Under the circumstances, it is important that care is exercised in the formulation of the absorbing conditions and the matter should be further investigated. The only way to avoid numerical errors entirely is to know in advance the angle of incidence of the wave at the boundary, however this is unlikely to be the case in real situations. One method by which this can be overcome, where an absorbing boundary is required is to use the sponge layer technique which was described in section 3.2.

It remains to consider boundary conditions which represent partially or totally reflecting structures. In this case a boundary condition similar to (4.7) can be derived which includes a reflection coefficient. For incident waves at 45° it will take the form,

$$u_{i+1}^{n+\frac{1}{2}} = (1-R)\left(u_{i+1}^{n-\frac{1}{2}} - \frac{Cr}{\sqrt{2}}\left(u_{i+1}^{n-\frac{1}{2}} - u_{i}^{n-\frac{1}{2}}\right)\right) \qquad (4.8)$$

where R is the reflection coefficient. For R = 1 we have total reflection, and for R = 0 total absorption (as in (4.7)).

In a numerical model harbour boundaries will be represented in a stepwise manner. It needs to be demonstrated that the reflective properties of these boundaries are accurately modelled when conditions similar to (4.8) are applied. With this in mind we examine the case where a solitary wave travelling from left to right is incident on a reflecting boundary at 45° to the incident wave angle. If the reflection of the wave is total, then, its direction afterwards should change by 90°, this case is illustrated in Figure 20. It can be seen that despite its stepwise representation in the model, the boundary does reflect the wave correctly. In particular, at the boundary the wave height is doubled and the part of the wave which has not reached the boundary continues to propagate undisturbed.

As a further test, the orientation of the wall is altered from 45° to 60°, the direction of the wave after reflection is again found to be correct (see Fig 21). It would appear from these test that despite the stepwise representation the reflective properties of the boundaries of the finite difference scheme are still accurately modelled. Finally, for the same

test we introduce a reflection coefficient R at the wall. For the results shown in Figure 22 this coefficient is taken equal to 1/2 whereas in Figure 23 it is taken simply as 0 ie the boundary is fully absorbing. The boundary conditions which are applied correspond to an angle of incidence of 0°. It can be seen that for both cases the boundary conditions demonstrate the expected properties that is, in Figure 22 the height of the wave reflected from the wall is half that of the incident height. Whereas, in Figure 23 no reflected wave is evident.

4.3 Wave diffraction by breakwaters

Having demonstrated that the numerical model will represent the effects of wave reflections and absorption at its boundaries, it remains to check that wave diffraction by breakwaters is modelled correctly. For non-linear wave there is no theoretical solution against which the model results can be checked. Therefore, the approach which was taken was to compare the results from the numerical model with those from physical model tests (see Ref 21). These physical model tests were primarily carried out to investigate the diffraction of set down. However, in obtaining this data results on the diffraction of ordinary waves were obtained and these can be used for the comparisons given here.

The numerical model was set up to represent the layout of the physical model, which is shown in plan in Figure 24. The depth throughout the harbour was 25m. The numerical model was run with an incident sine wave of frequency 0.03Hz and amplitude 0.023m, this corresponded to one of the tests carried out in the physical model. The numerical model for this case used a grid size Δx = 15m with a time step of 0.66s giving a Courant number of 0.69. The physical model test results were given in the form of diffraction coefficients at positions 1 to 7 (see Fig 24), which are on 15° radials from the breakwater at a distance r from the tip. In this case r = 513m, which is approximately the wavelength of the incident wave.

A comparison of the diffraction coefficients positions 1 to 7 for both the physical and numerical models is given in Figure 25. Also in Figure 25, for comparison wave conditions from a linear numerical model (described in Ref 22). It can be seen from Figure 25

that the results from the physical and numerical models are in reasonably good agreement, being within 5-10% of each other at all locations. This means that diffraction of a regular sine wave is correctly represented in the numerical model. It is also interesting to note that the linear model gives slightly higher values of the diffraction coefficient than either the present numerical model or the physical model (both of which are non-linear) at positions directly exposed to the incident wave (positions 6 and 7). But, that the linear diffraction coefficients are lower than both the present model and the physical model at the positions in the shelter of the breakwater.

Having demonstrated that the numerical model gives a good representation of diffraction of a single incident sine wave by a breakwater it remains to consider diffraction of a regular wave group with its associated set down.

4.4 Set down wave tests

A description of the theory was given in section 3.3.1, and it was shown in section 3.3.2 that the Boussinesq model would represent set down amplitudes in one dimension to within ±20%. It remains to show that two dimensional effects, and in particular diffraction of set down, can be modelled correctly.

To investigate the ability of the numerical model to represent diffraction of wave groups a series of comparisons were made between its results and the results from a series of physical model tests (Ref 21). The numerical model layout used was the same as for the physical model, see Figure 24. The tests in the numerical model were carried out for incident waves with the following characteristics:

	Frequency (Hz)	Amplitude (m)	Wavelength (m)
Primary wave one	0.07	1.65	202
Primary wave two	0.10	1.97	128
Set down	0.03	0.23	513*

(*Wavelength of a free wave at the set down frequency).

These incident conditions correspond to those used in one of the physical model tests described in Ref 21. As discussed in section 3.3.2 the set down wave amplitude will differ in the physical and numerical models, in the physical model the set down wave amplitude is 0.28 m for this combination of primary waves.

The mathematical model was run using a grid size Δx = 15m and a time step Δt = 0.66s, giving a Courant number of 0.69. This means that for the shortest primary wave there were approximately 8.5 points per wave length. During the mathematical model run the surface elevation data are stored as a time series at grid points which correspond to physical model probe positions. The time series are then analysed to give wave ampulitudes at the various frequencies for each probe position. The positions which were used are at distances 0.5L, 0.7L and L from the breakwater tip, where L = 513m is the wavelength corresponding to the beat frequency f_- = 0.03, along lines positioned at 15°, 30°, 45°, 60°, 75° and 90° from the breakwater (see Fig 24). The results for both the physical and numerical model are presented as diffraction coefficients at the various positions. (The diffraction coefficient is defined as ratio the amplitude of the diffracted wave to the amplitude of the incident wave at the breakwater tip).

The first comparison which was made between the results from the two models was for the diffraction coefficients at L from the tip for waves at the primary and set down frequencies; these results are given in Figure 26. It can be seen that the two sets of results are in good agreement at the set down frequency, with the same trend being displayed in the numerical model as in the physical model results. For the primary frequencies agreement is also good except at positions 1 and 2 for 0.07Hz, and position 1 for 0.10Hz. One explanation for the differences at these locations is the presence of the breakwater. It is possible that in the numerical model some energy is being reflected back into the model area by the breakwater and that this is contaminating the results at positions 1 and 2.

A further comparison between the numerical and physical model results was made for the diffractions coefficients at the set down frequency at locations 1 to 7 at 0.5L, 0.7L and L from the breakwater tip, these results are shown in Figure 27. Again the two sets of results for all of these locations are in good agreement. Finally, in Figure 28 a comparison is presented of the set down wave diffraction coefficients, and those of a free wave at the same frequency for both the physical and numerical models. It is clear from Figure 28 that the numerical model gives the same trends which were evident in the physical model. At most positions the agreement between the two sets of results is good, although the mathematical model diffraction coefficients are lower than the physical model values at all positions for both the free wave and the set down wave. The behaviour of the set down wave at these locations is only similar to that of the free wave at positions well inside the shelter of the breakwater.

From the results given above we conclude that the numerical model gives an accurate representation of diffraction of set down.

5 CONCLUSIONS AND RECOMMENDATIONS

5.1 Conclusions

A finite difference scheme has been developed which gives a mathematical solution to the Boussinesq wave equation for water of constant depth. The finite difference scheme was implemented on the DAP computer as a predictor-corrector method. The resulting mathematical model was found to provide accurate numerical solutions to the Boussinesq equations. In particular, it represents well the propagation of linear and non-linear waves in shallow water, taking into account both reflection and diffraction effects. The model also successfully reproduced propagation and diffraction of set down beneath regular wave groups.

5.2 Recommendations

The work described in this report is the first stage in the development of a finite difference model to some the Boussinesq equations. To develop the model further to allow more realistic harbour layouts to be represented it is recommended that:

(a) The model should be extended to include varying depth terms, thereby allowing refraction effects to be represented

(b) Random and multi-direction incident waves should be included in the model.

(c) Boundary conditions should be investigated further, so that more realistic harbour

boundaries, eg rubble mound breakwaters, can be modelled accurately.

(d) A series on physical model tests should be undertaken to provide data against which the model including developments (a) to (c) can be tested.

6 ACKNOWLEDGEMENTS

The authors would like to thank colleagues in the Maritime and Tidal Engineering Departments of Hydraulics Research for their useful discussions. In particular, thanks are due to Dr S W Huntington for his help and encouragement.

7 REFERENCES

1. Stoker J J. Water waves. Interscience New York 1957.

2. Boussinesq J. Théorié générale des movements qui sort 3 propagés dans un canal rectangulaire horizontal. C R Lebd Séanc Acad. Sci. Paris. 73 p256-260. 1871.

3. Peregrine D H. Long waves on beach. Journal of Fluid Mechanics, Vol 27, Part 4, 1967.

4. Witham G B Linear and non-linear waves. John Wiley and Sons, 1974.

5. Mc Cowan A D. Numerical Simulation of water waves. Proc. 4th Australian Conference on Coastal and Ocean Engineering, Adelaide, November 1978.

6. Abbot M B, Petersen H M and Skovgaard O. On the numerical modelling of short waves in shallow water. Journal of Hydraulic Research 16 No 3 1978.

7. Mc Cowan A D. Development in numerical short wave computations. Proc 5th Australian conference on Coastal and Ocean Engineering. Perth, November 1981.

8. Larsen J and Dancy H. Open boundaries in short wave simulation- a new approach. Coastal Engineering 7 p 285-297 1983.

9. Abbot M B, the Cowan A D and Warren I R. Accuracy of short wave numerical models. ASCE

Journal of Hydraulic Engineering. Vol 110 No 10 1984.

10. Madsen P A and Warren I R. Performance of a numerical short wave model. Coastal Engineering 8 p 73-93. 1984.

11. Hauguel A. A numerical model of storm waves in shallow water. Proc. 17th. Int Cont on Coastal Engineering Vol 1 p 746-762 Sydney, Australia 1980.

12. Schaper H and Zielke W. A numerical solution of Boussinging type wave equations. Proc. 19th Int Conf on Coastal Engineering Vol II p 1057-1072 Houston, U.S.A. 1984.

13. Rottmann-Sode W, Schaper M and Zielke W. Two numerical wave models for harbours. Proc. BHRA Int Cont on Numerical and Hydraulic Modelling of Ports and Harbours. Birmingham, England 1985.

14. Prüser H-H, Schaper H and Zielke W. Irregular wave transformation in a Bossinesq wave model. Proc 20th Int Conf on Coastal Engineering Taipei, Taiwan 1986.

15. HRS tidal modelling system. Hydraulics Research Report IT 239. 1982.

16. Galvin C J Jnr. Finite amplutude, shallow water waves of periodically recurring form. CERC report 5-72. 1970.

17. Madsen OS Mei SS and Savage RP. The evolution of time periodic long waves of finite amplutude. Jounal of Fluid Mechanics, Vol 44, Part 1 1970.

18. Longuet - Higgins M S and Stewert R W. Deep Sea Reserch Vol 11.

19. Bowers E C. Harbour resources due to set down beneath wave groups. Journal of Fluid Mechanics, Vol 79. 1977.

20. Bowers E C. Long period disturbances due to wave groups. Proc 17th Int Conf Coastal Engineering, Sydney 1980 Vol 1 p 610.

21. Bowers E C and Beresford P J Diffraction of set down waves in harbours: laboratory work using regular wave groups. Hydraulics Research Report IT283, September 1984.

22. Smallman J V. The application of a computational model for the optimisation of harbour layout. Proc 2nd Int Cont on Coastal and Port Engineering in Developing Countries (COPEDEC). Bejing, China. September 1987.

TABLES.

TABLE 1: **Amplitudes of sine wave at positions along a wave flume. Water depth = 25m, wave amplitude 1.61m, period 14s.**

Distance from paddle (m)	Wave amplitude (m) at frequency 0.07Hz		
	Without sponge layer	With sponge layer	
		5 cells wide	10 cells wide
770	1.53	1.61	1.61
898	1.64	1.63	1.61
1155	1.51	1.61	1.61
1283	1.79	1.62	1.61
1412	1.47	1.62	1.61
1540	1.79	1.61	1.61
1668	1.63	1.60	1.61
1797	1.42	1.61	1.61
1850	1.80	1.61	1.61

TABLE 2: Amplitudes of cnoidal wave at positions along a wave flume. Water depth = 25m, wave amplitude 1.60m, period 14s.

Distance from paddle (m)	Wave amplitude (m) at frequency 0.07Hz		Wave amplitude (m) at frequency 0.14Hz	
	without spong layer	with sponge layer	without sponge layer	sponge layer 10 cells wide
770	1.54	1.60	0.14	0.16
898	1.53	1.60	0.14	0.16
1155	1.51	1.60	0.15	0.14
1283	1.76	1.60	0.15	0.15
1412	1.42	1.60	0.15	0.15
1540	1.82	1.60	0.15	0.16
1668	1.66	1.60	0.14	0.15
1797	1.41	1.60	0.14	0.14
1850	1.85	1.60	0.16	0.15

TABLE 3: Sponge layer tests for regular wave group with primary frequencies 0.07Hz and 0.10Hz. Water depth 25m, x = 15m, t = 0.66s. Expected wave amplitudes are 0.23m at f- =0.03Hz, 1.65m at f = 0.07Hz and 1.97m at f = 0.10Hz.

Distance from paddle (m)	Ampltudes at specified frequencies (m)								
	No sponge layer			10 cell sponge layer			20 cell sponge layer		
	f=0.03Hz	f=0.07Hz	f=0.10Hz	f=0.03Hz	f=0.07Hz	f=0.10Hz	f=0.03Hz	f=0.07Hz	f=0.10Hz
15	0.37	1.58	1.89	0.22	1.50	1.92	0.22	1.56	1.92
315	0.27	1.58	1.94	0.23	1.51	1.94	0.23	1.51	1.94
615	0.29	1.61	2.02	0.17	1.49	1.96	0.17	1.49	1.96
915	0.25	1.66	2.02	0.31	1.49	1.93	0.31	1.50	1.93
1215	0.21	1.57	2.04	0.19	1.49	1.95	0.19	1.49	1.96
1515	0.15	1.51	1.93	0.17	1.50	1.97	0.17	1.50	1.97
1815	0.19	1.50	1.96	0.21	1.54	1.90	0.21	1.54	1.90
2115	0.28	1.51	1.75	0.18	1.52	1.75	0.18	1.52	1.75

TABLE 4: Sponge layer tests for regular wave group with primary frequencies 0.07Hz and 0.10Hz. Water depth 25m, Δx = 12.5m, Δt = 0.55s. Expected wave aplitudes 0.23m at f- = 0.03Hz, 1.65m at f = 0.07Hz and 1.97m at f = 0.10Hz.

Distance from paddle (m)	Amplitudes at specified frequencies (m)								
	No sponge layer			10 cell sponge layer			20 cell sponge layer		
	f=0.03Hz	f=0.07Hz	f=0.10Hz	f=0.03Hz	f=0.07Hz	f=0.10Hz	f=0.03Hz	f=0.07Hz	f=0.10H
25	0.28	1.51	1.81	0.23	1.56	1.89	0.22	1.56	1.8
775	0.33	1.64	1.84	0.20	1.52	1.88	0.20	1.52	1.8
900	0.25	1.56	1.85	0.23	1.55	1.92	0.23	1.55	1.9
1163	0.33	1.58	1.82	0.23	1.50	1.86	0.23	1.51	1.8
1288	0.26	1.64	1.95	0.21	1.60	1.96	0.21	1.60	1.9
1413	0.34	1.60	1.95	0.20	1.54	1.91	0.20	1.54	1.9
1538	0.18	1.55	2.03	0.22	1.50	1.89	0.22	1.49	1.8
1663	0.29	1.43	2.01	0.18	1.53	1.90	0.18	1.52	1.9
1800	0.32	1.51	1.86	0.18	1.51	1.83	0.18	1.52	1.8

TABLE 5: Mesh size variation tests for regular wave group with primary frequencies 0.07Hz and 0.10Hz. Water depth 10m. Expected wave amplitudes are 0.075m at f = 0.03Hz, 0.3m at f = 0.07Hz and 0.5m at f = 0.10Hz.

15m mesh spacing

Dist from paddle (m)	Ampltudes (m) at f=0.03Hz	f=0.07Hz	f=0.10Hz
15	0.083	0.29	0.48
90	0.068	0.28	0.48
165	0.070	0.30	0.48
240	0.070	0.29	0.48
315	0.057	0.28	0.49
465	0.043	0.29	0.49
540	0.043	0.27	0.49
615	0.041	0.26	0.49
690	0.029	0.28	0.49
765	0.021	0.28	0.49

5m mesh spacing

Dist from paddle (m)	Ampltudes (m) at f=0.03Hz	f=0.07Hz	f=0.10Hz
5	0.076	0.27	0.49
25	0.082	0.28	0.49
50	0.077	0.28	0.49
75	0.072	0.26	0.50
100	0.083	0.27	0.49
150	0.073	0.26	0.48
200	0.076	0.27	0.46
250	0.079	0.28	0.47
500	0.069	0.28	0.48
750	0.075	0.28	0.47

TABLE 6: Amplitudes at the set down frequency for physical and numerical models. Regular wave group tests primary frequencies 0.07Hz and 0.10Hz, set down frequency 0.03Hz, L=513m. Expected set down amplitude for physical model 0.28m, for numerical model 0.23m.

Dist from paddle (wavelength)	Physical model	Numerical model 15m mesh	Numerical 12.5m mesh
3 L/2	0.31	0.27	0.20
7 L/4	0.27	0.29	0.23
9 L/4	0.28	0.32	0.23
5 L/2	0.28	0.20	0.21
11 L/4	0.28	0.19	0.20
3 L	0.25	0.25	0.22
13 L/4	0.27	0.20	0.18
7 L/2	0.28	0.20	0.18

FIGURES.

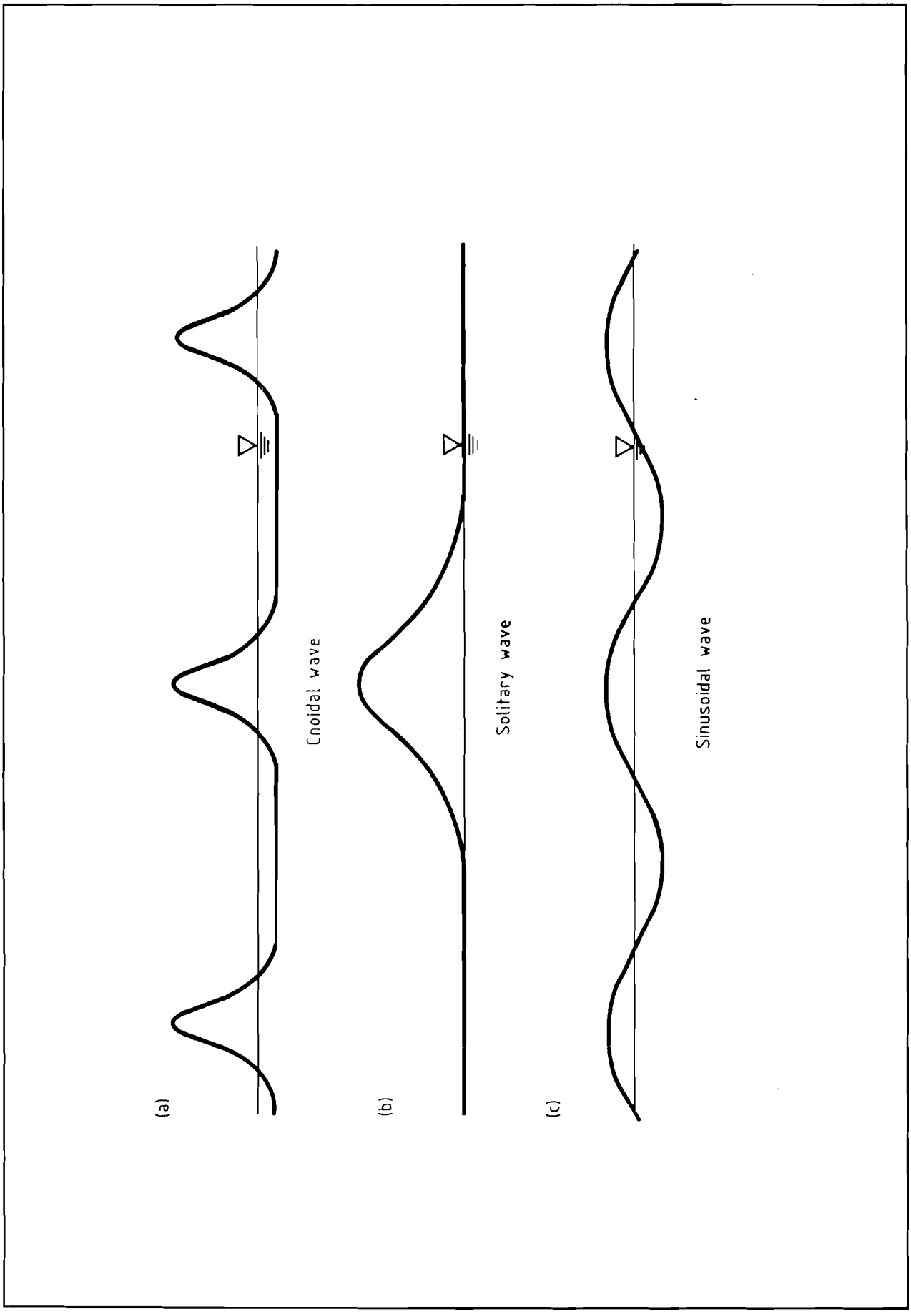

Fig 1 The cnoidal wave profile and its limiting forms

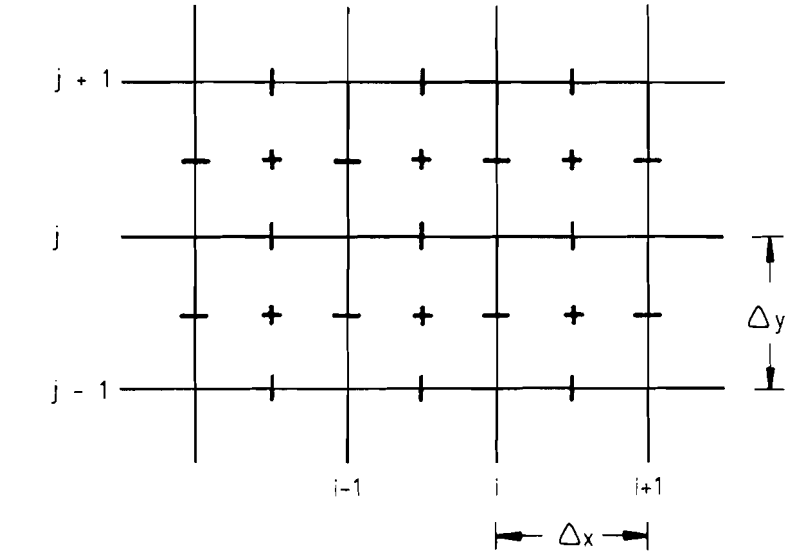

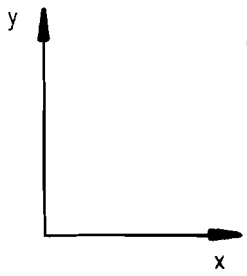

$\Delta x = \Delta y$

Key

+ elevation point

— u - point

| v - point

Fig 2(a) Grid layout in space

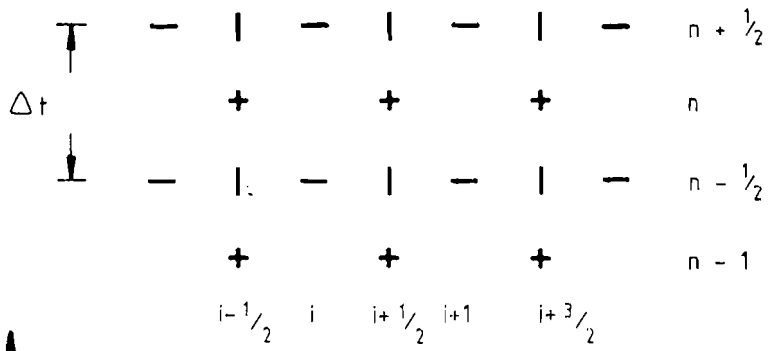

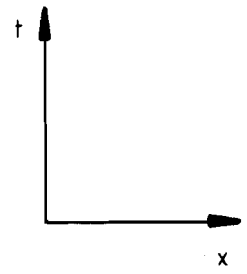

Fig 2(b) Grid layout in time

Fig 2 Basic finite difference grid

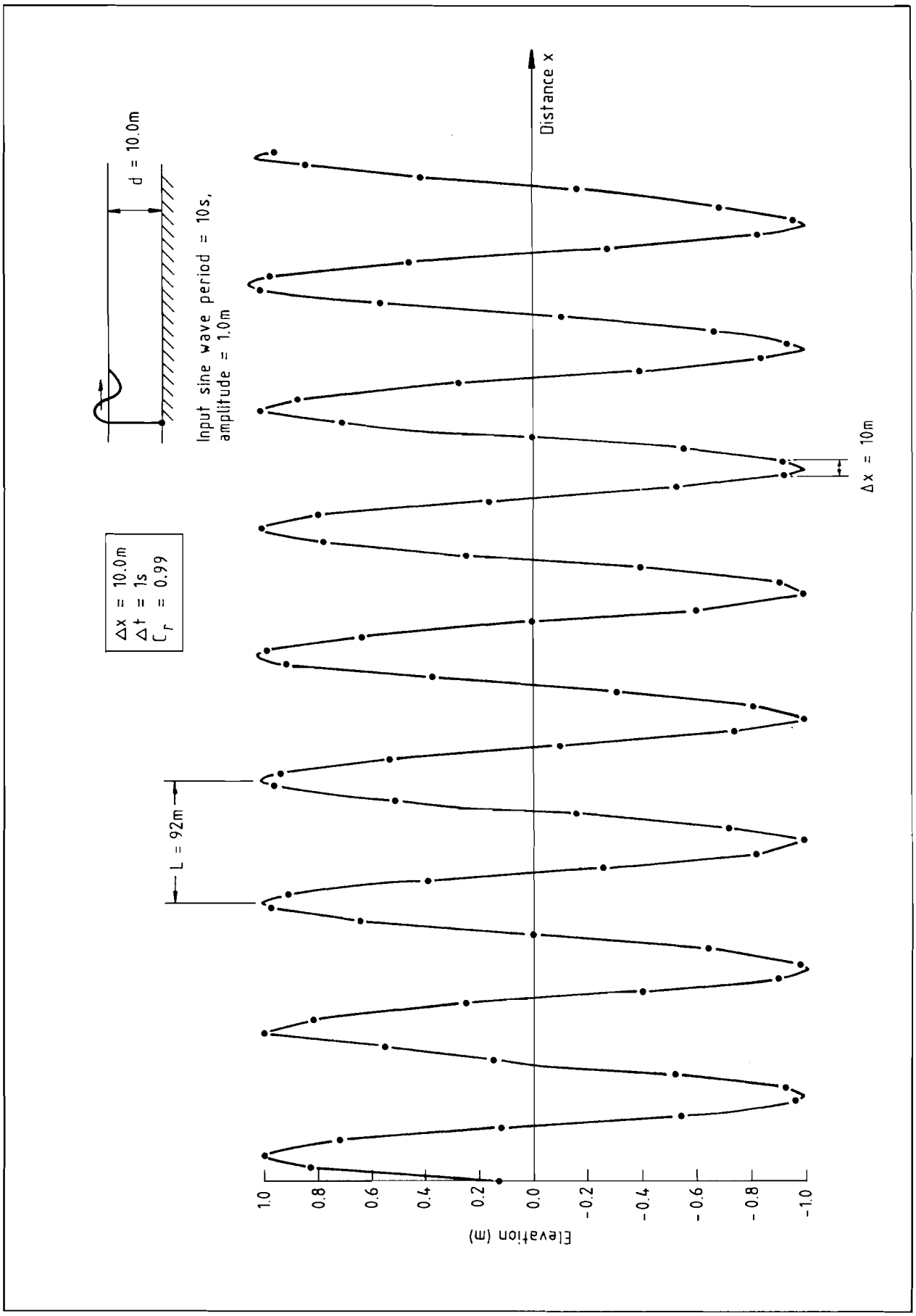

Fig 3 Reduction of wavelength due to dispersion - Linear implicit scheme

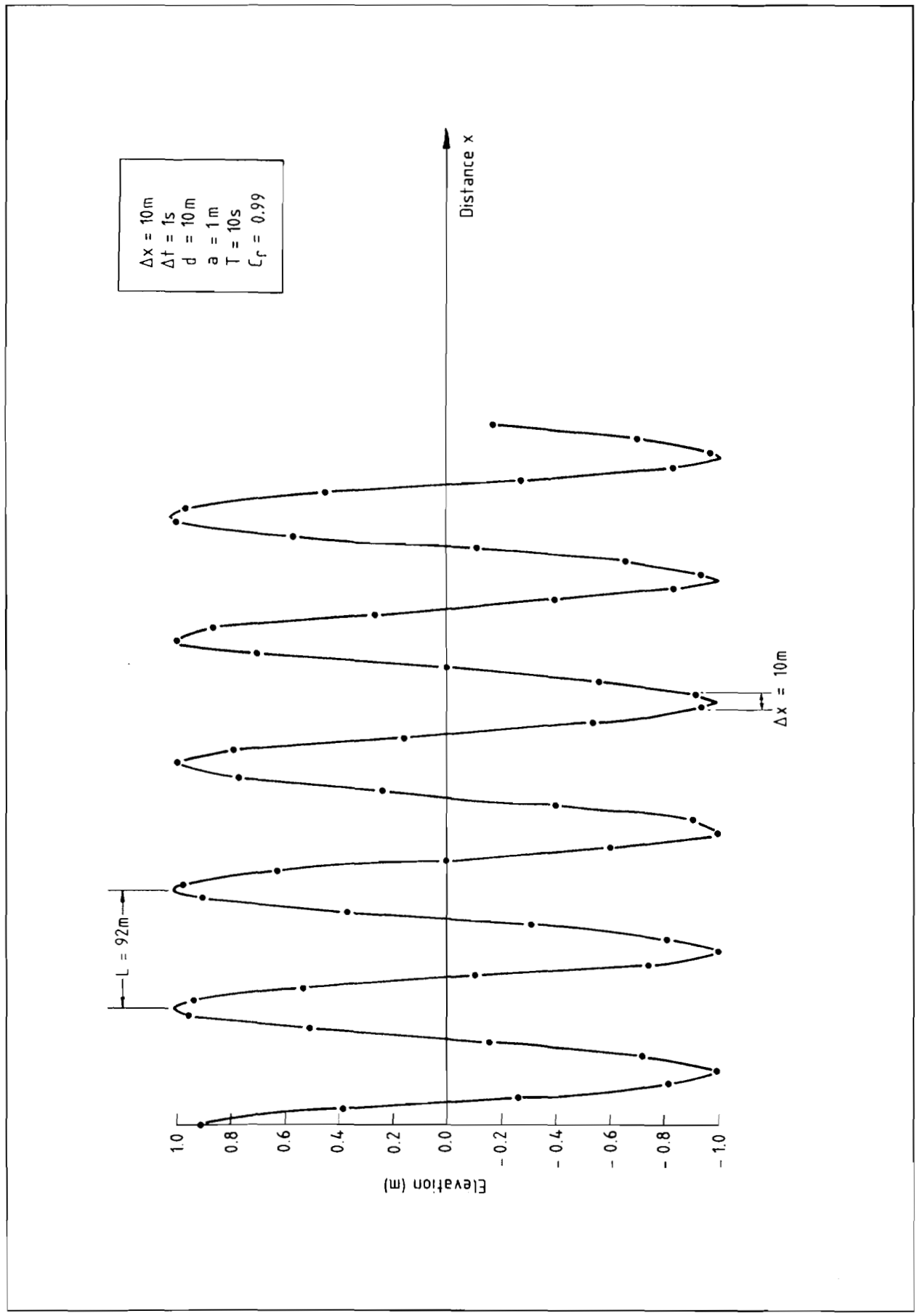

Fig 4 Reduction of wavelength due to dispersion - Predictor/corrector scheme

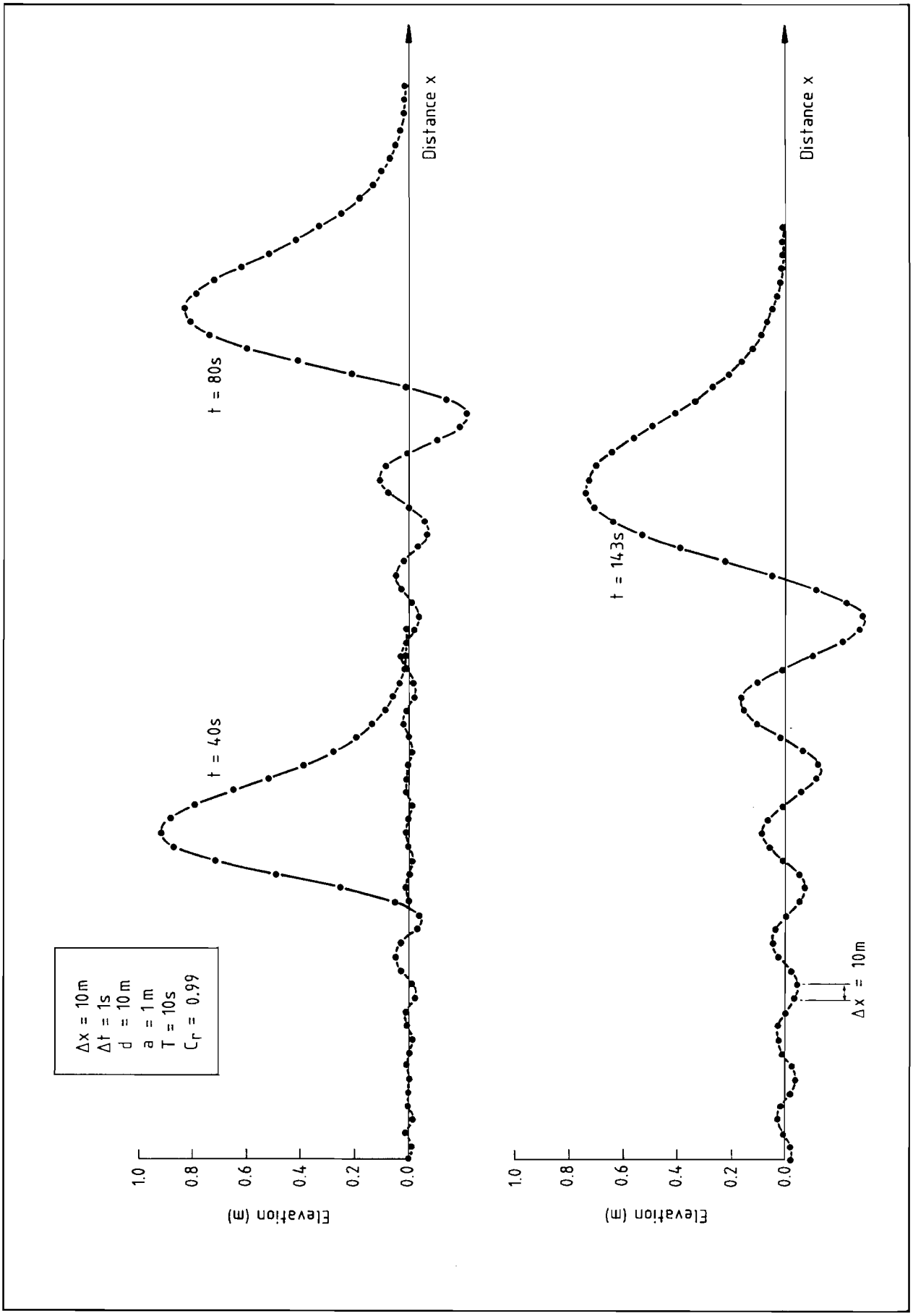

Fig 5 Dispersive evolution of a solitary wave

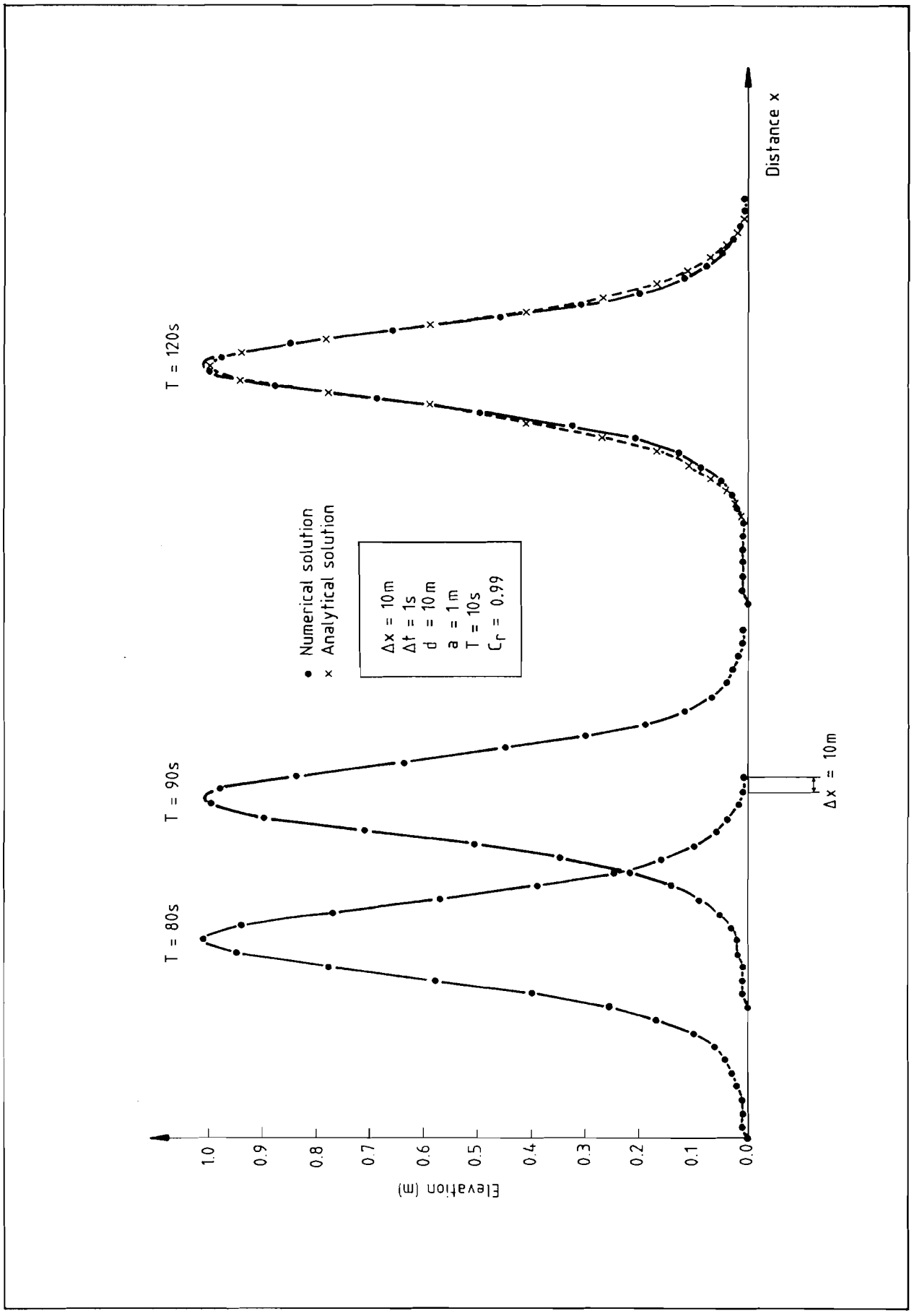

Fig 6 Travelling solitary wave - Implicit scheme

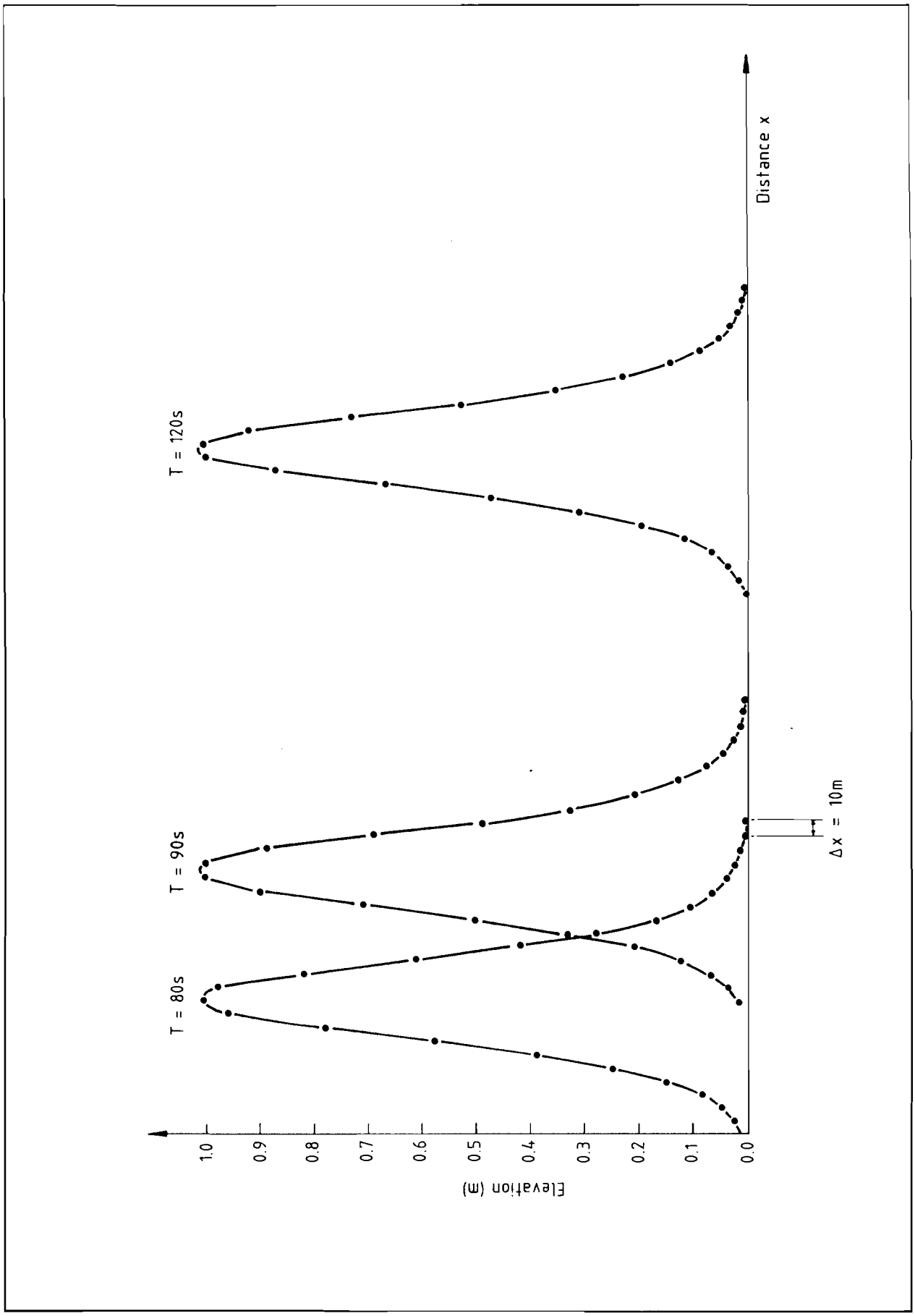

Fig 7 Travelling solitary wave - Predictor/corrector scheme

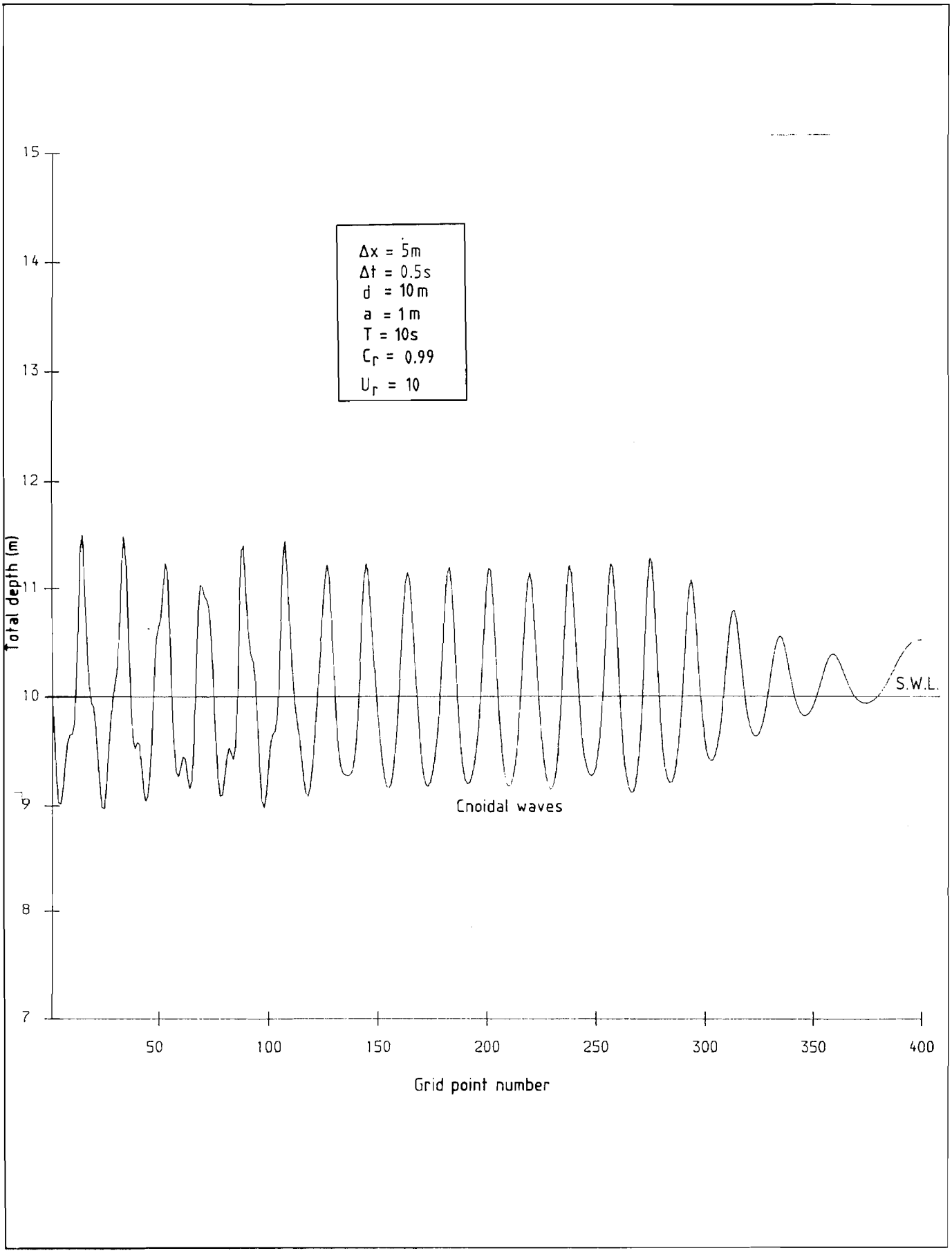

Fig 8 Production of cnoidal waves by a sine wave input

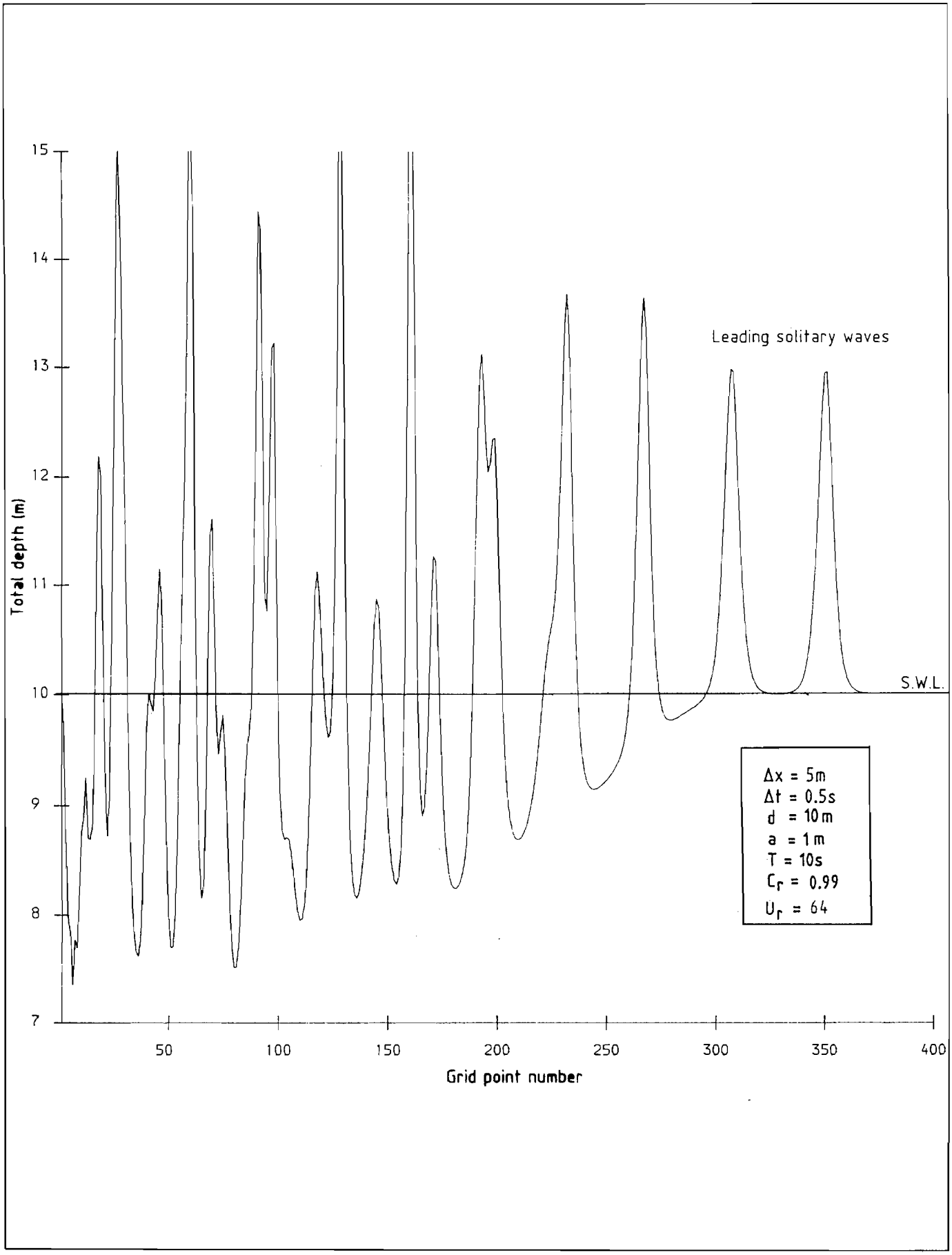

Fig. 9 Production of solitary waves by a sine wave input

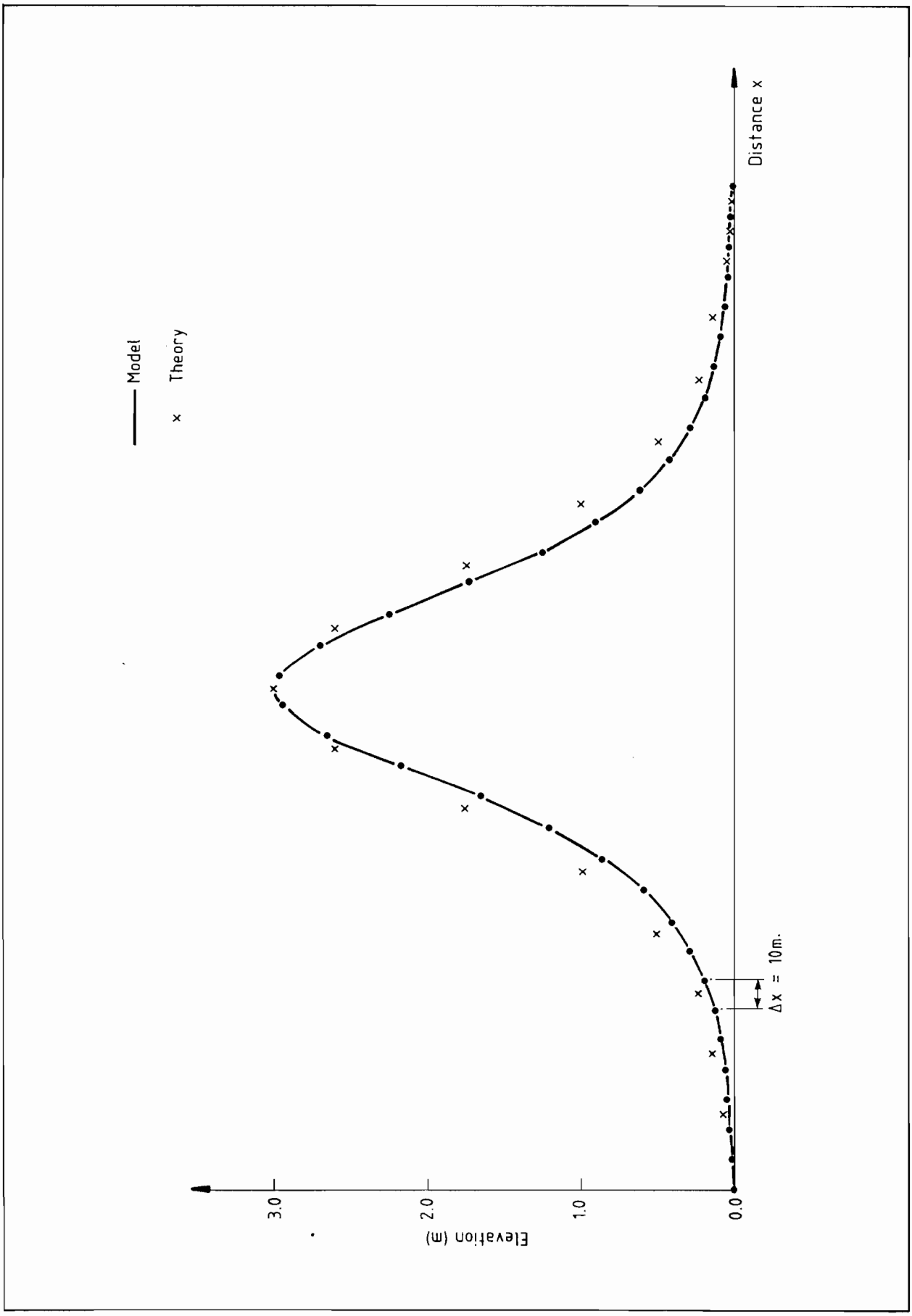

Fig 10 Comparison between model and theory - Solitary wave

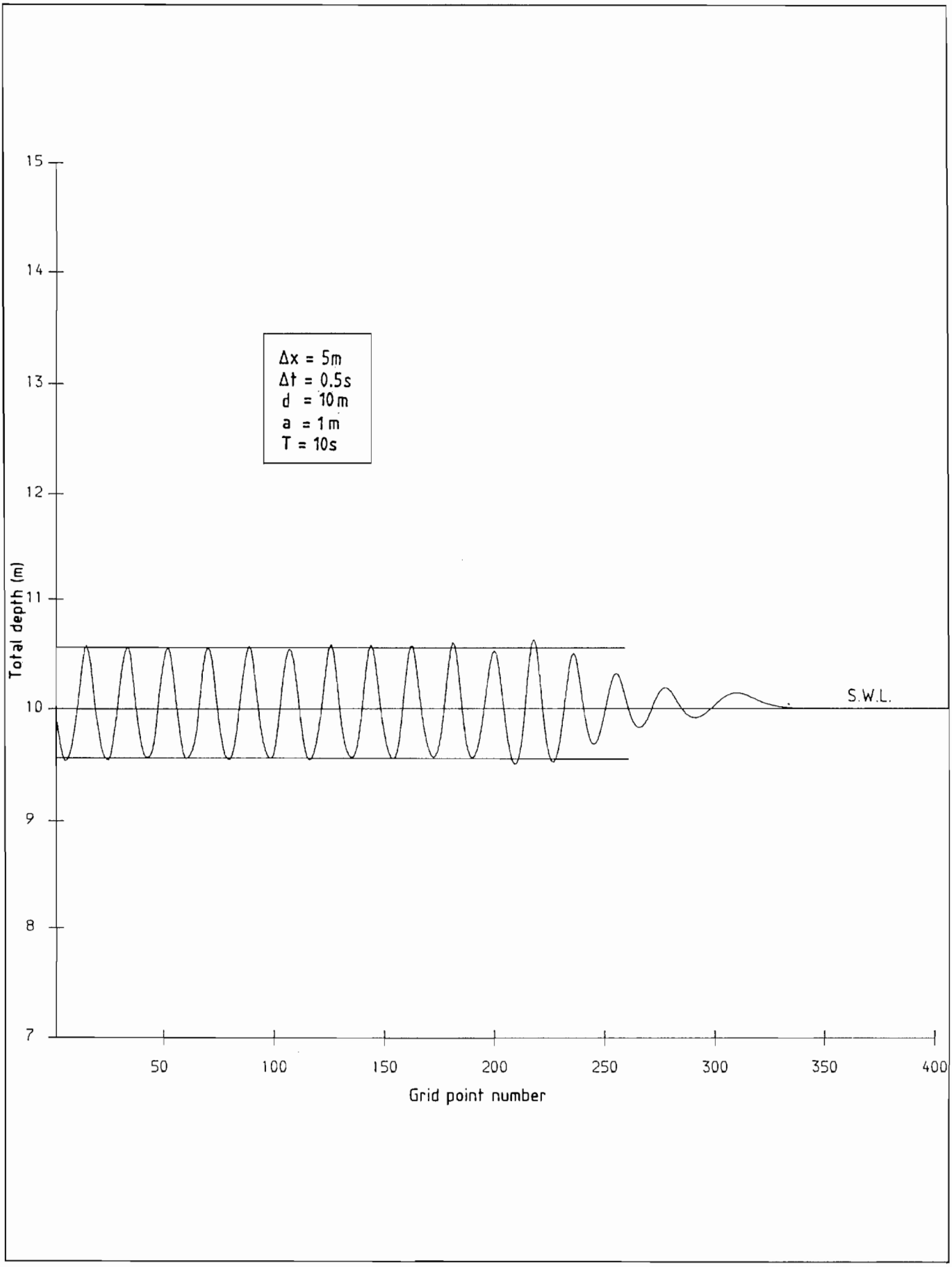

Fig 11 Cnoidal wave profile

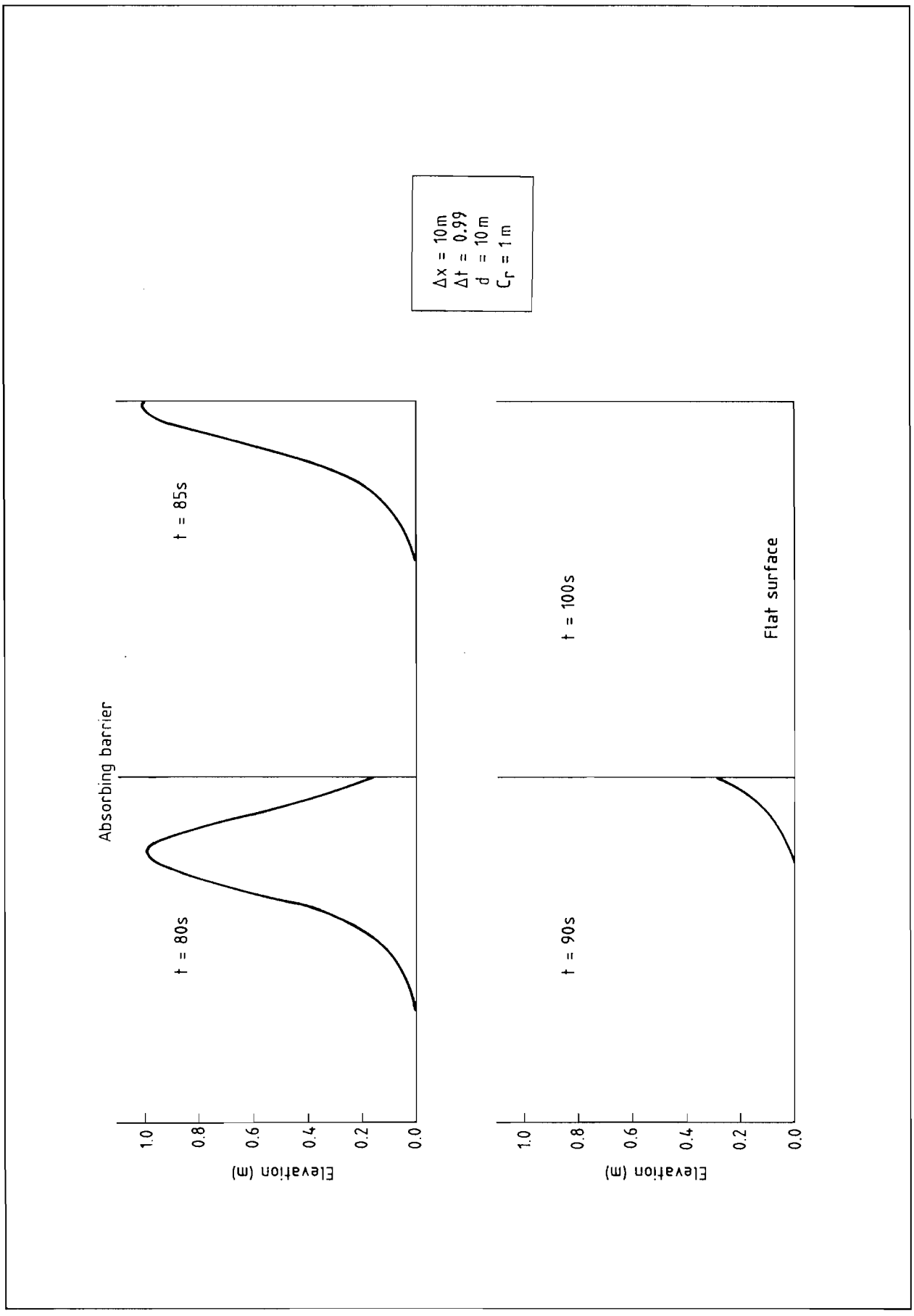

Fig 12 Absorption of a solitary wave - C_r = 1.0

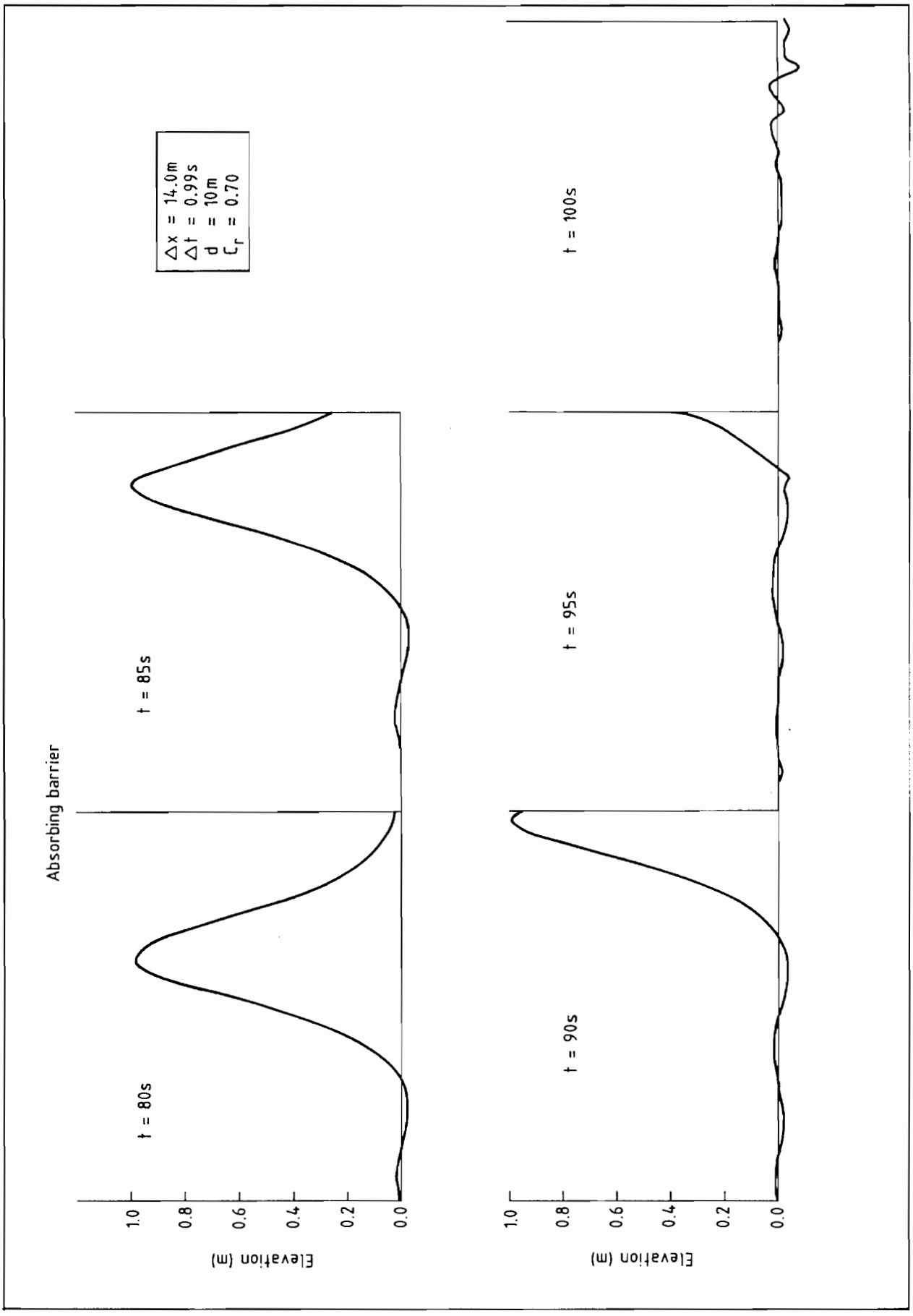

Fig 13 Absorption of a solitary wave - C_r = 0.70

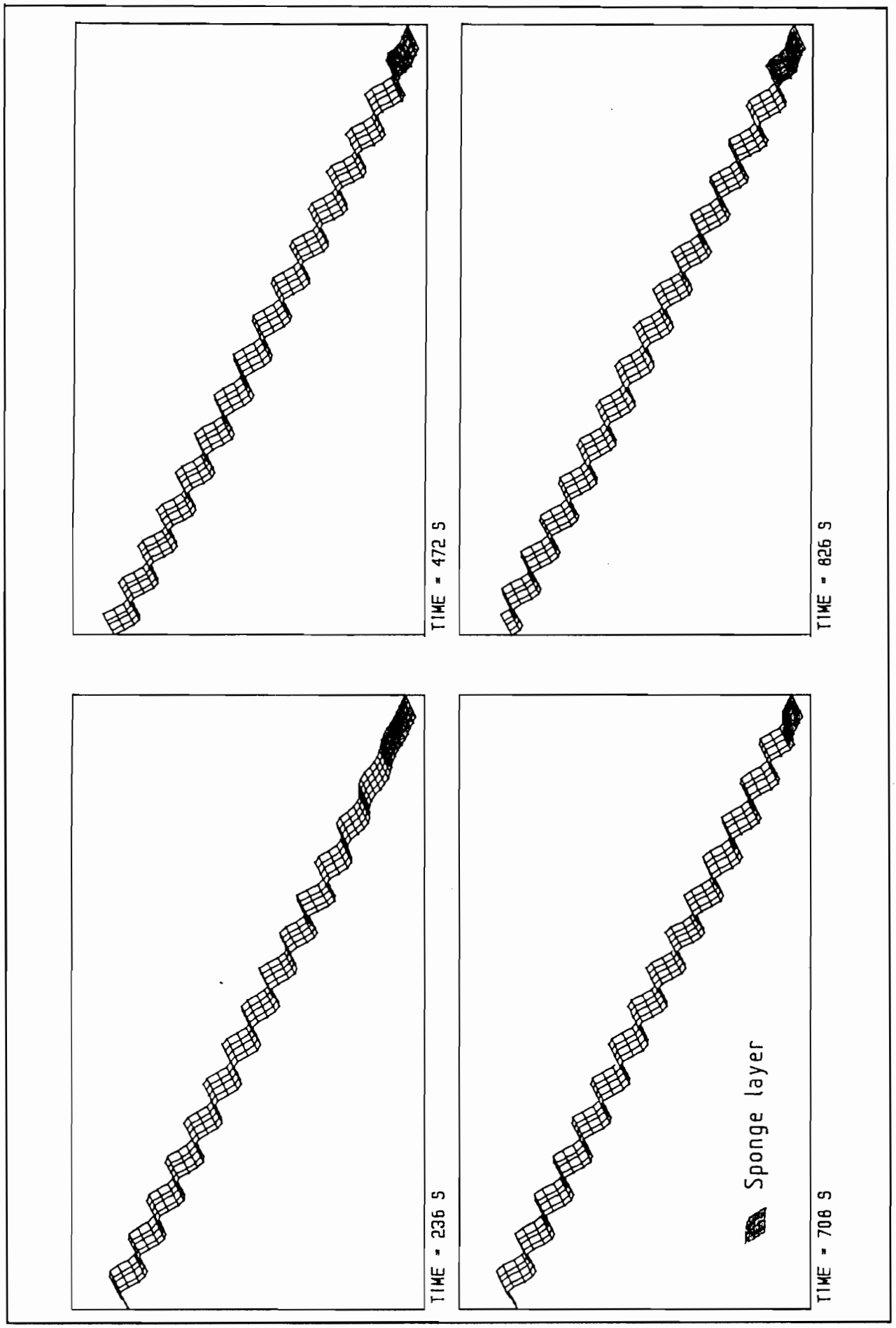

Fig 14 Cnoidal wave surface elevation, with sponge layer boundary conditions

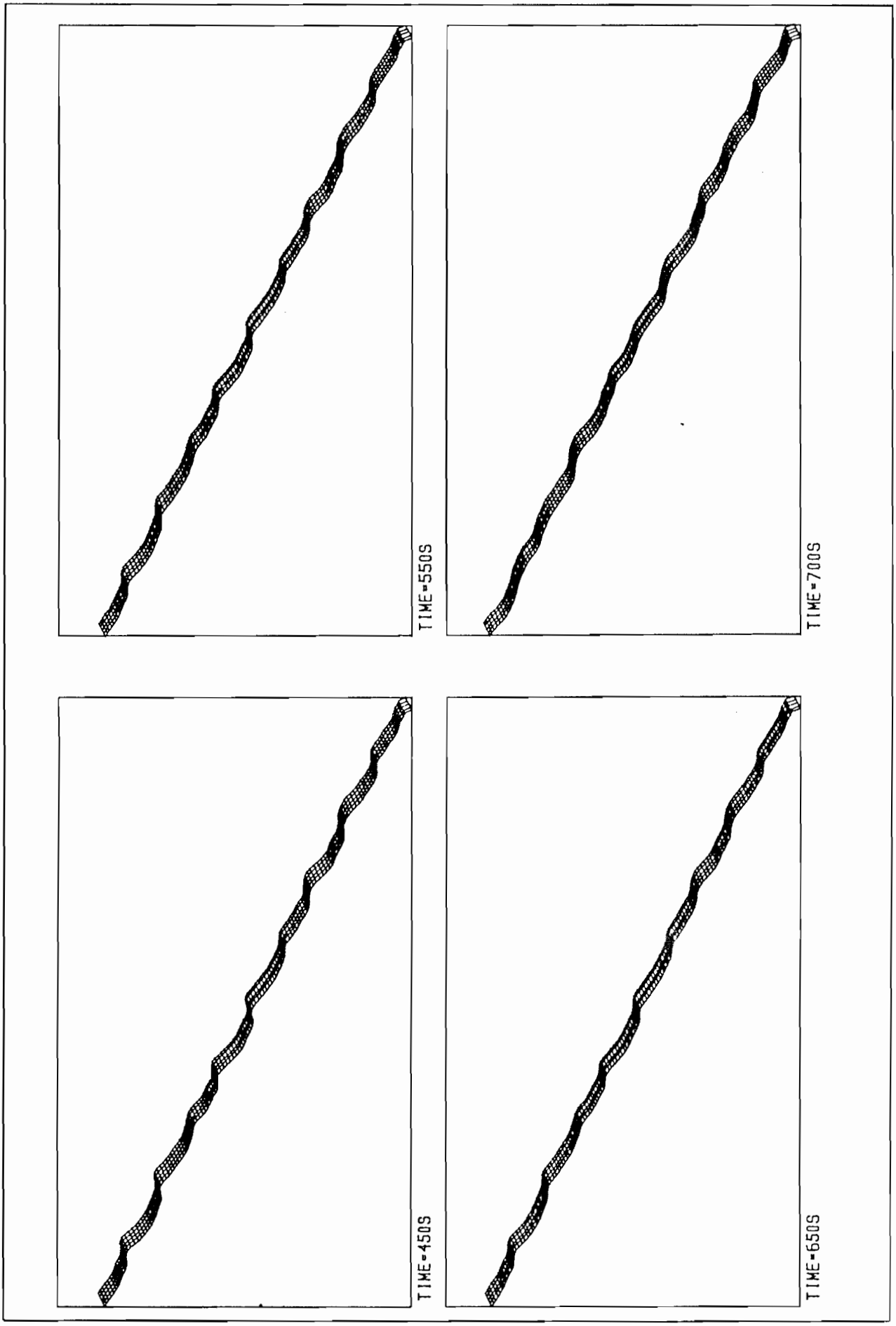

Fig 15 Two sine waves with associated set down waves,surface elevation.

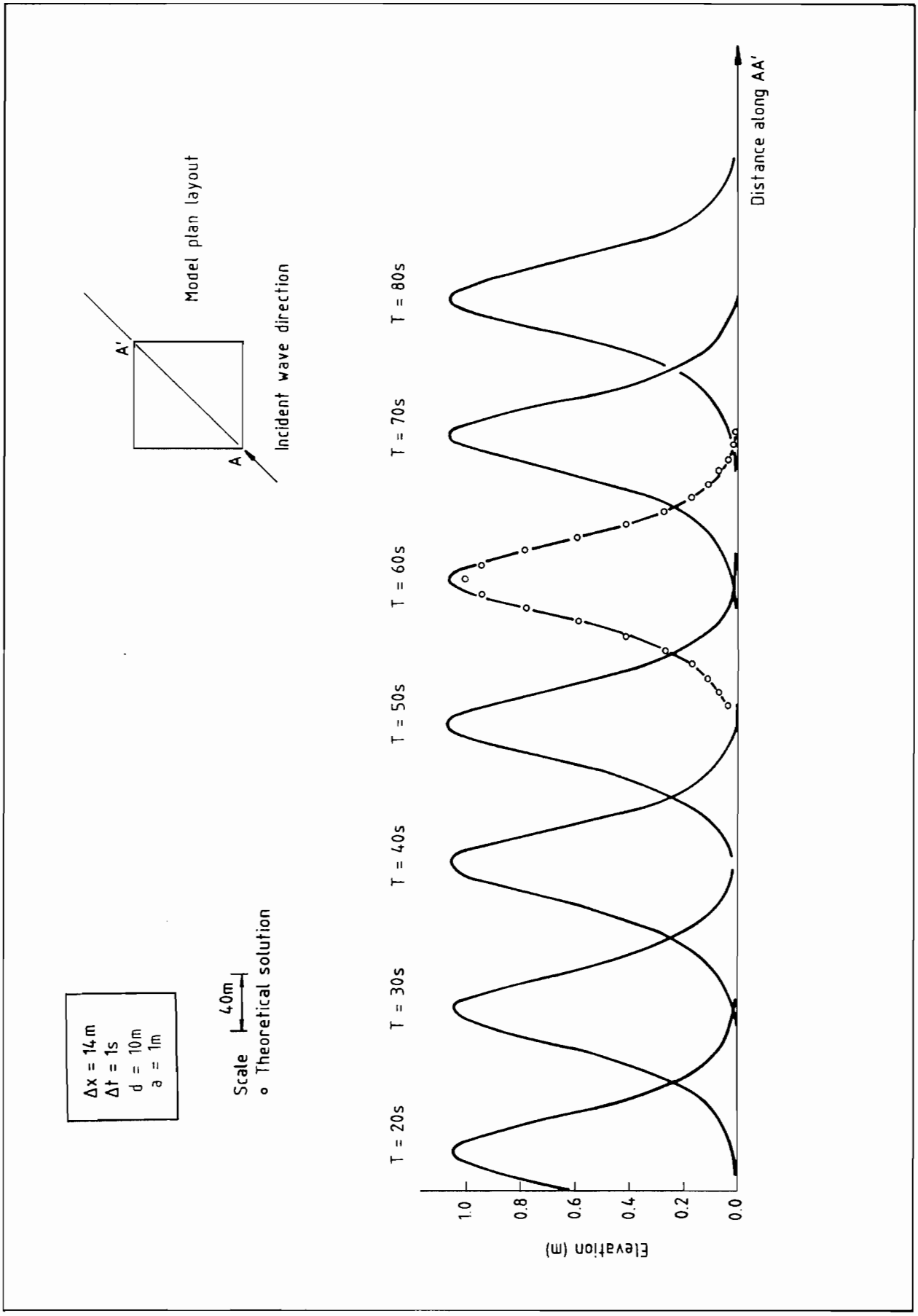

Fig 16 Propagation of a solitary wave at 45°

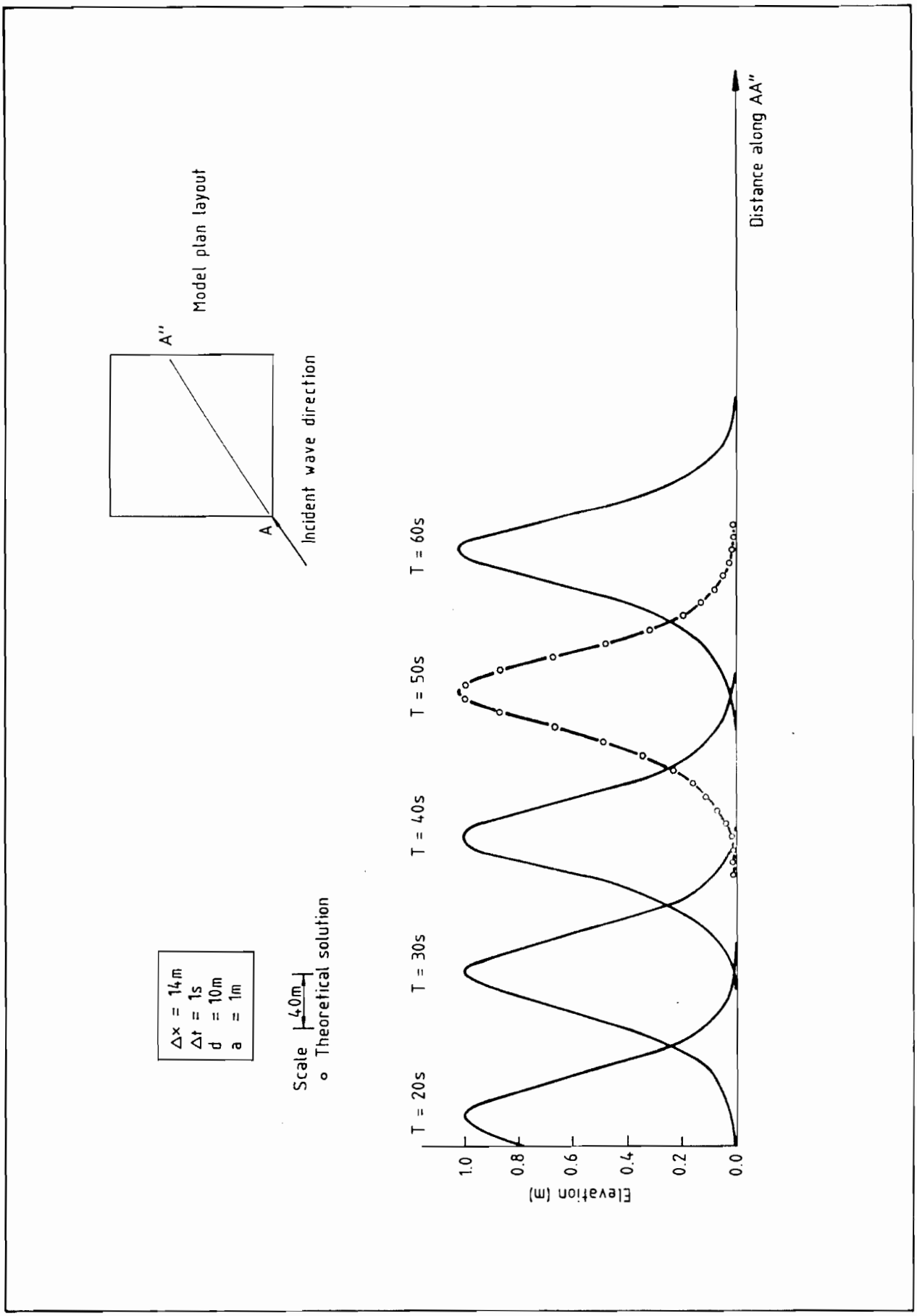

Fig 17. Propagation of a solitary wave at 30°

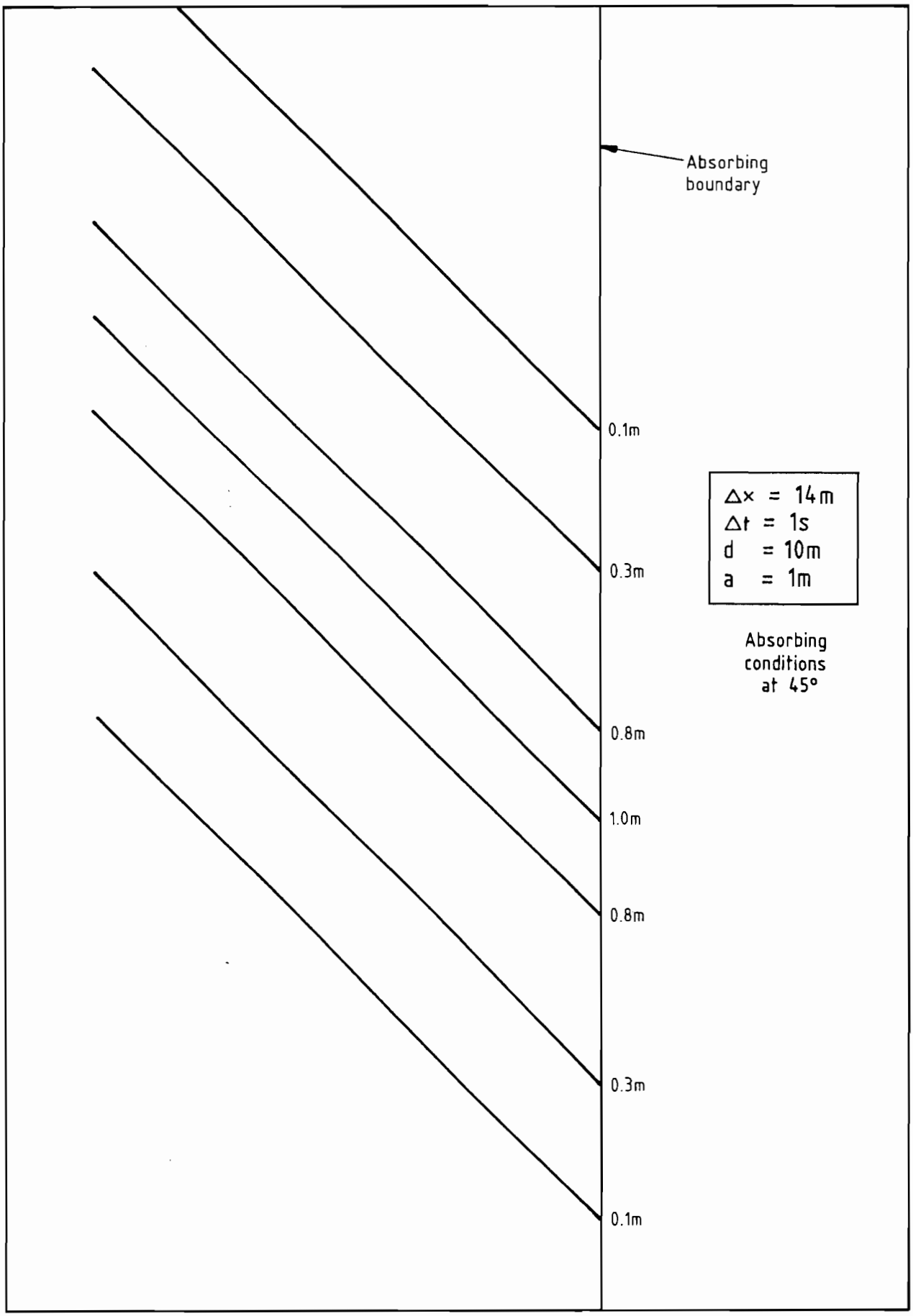

Fig 18 Surface elevation contours - propagation of a solitary wave at 45°

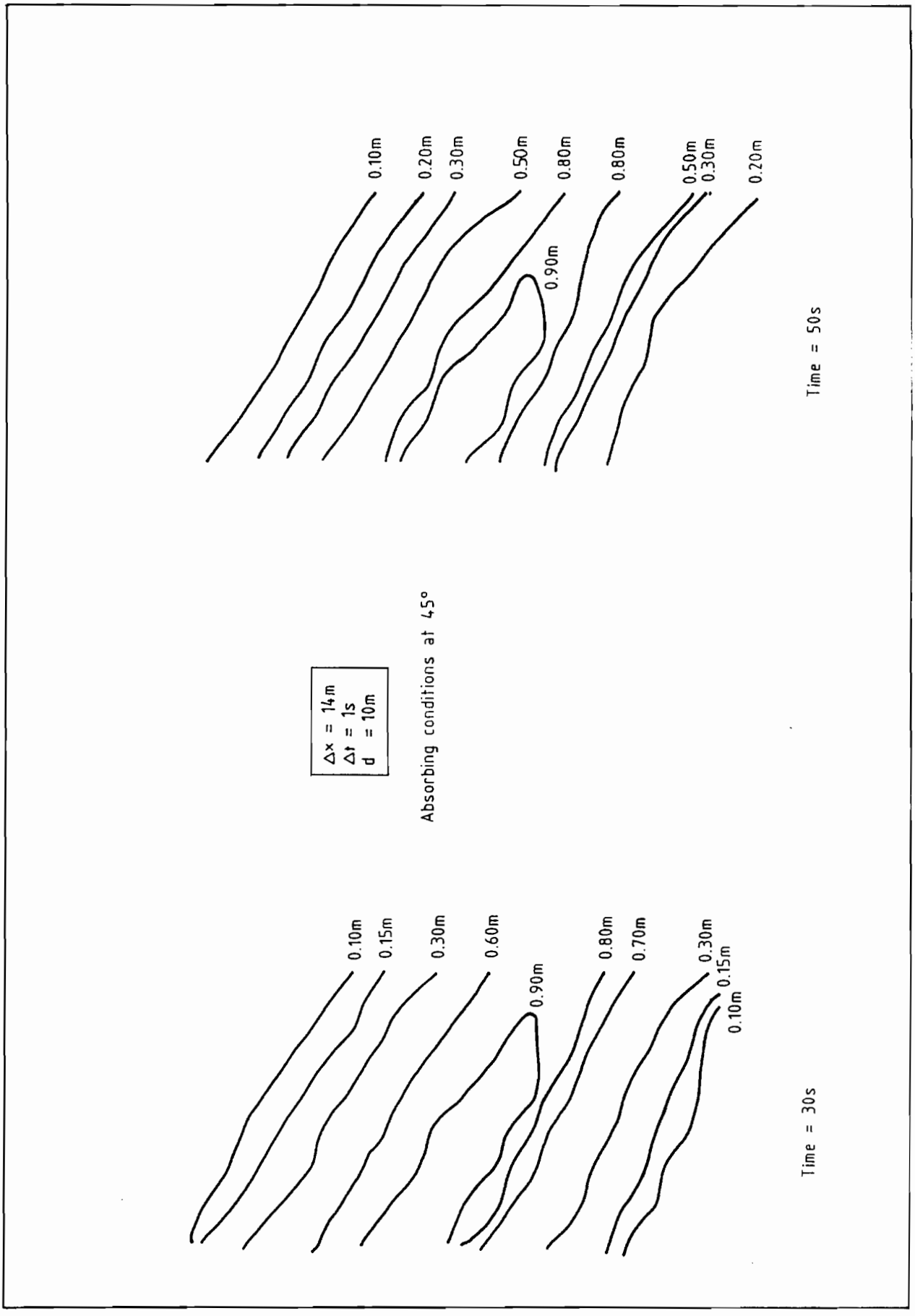

Fig 19 Surface elevation contours - propagation of a solitary wave at 60°

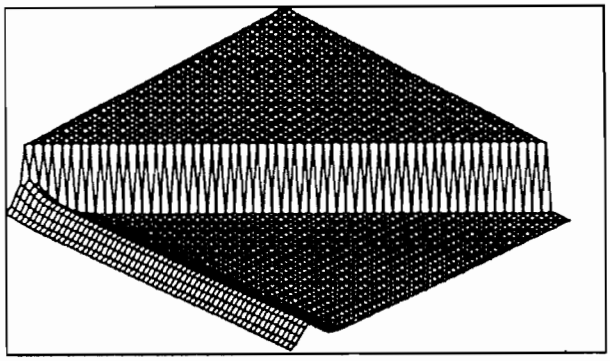

Time = 20s

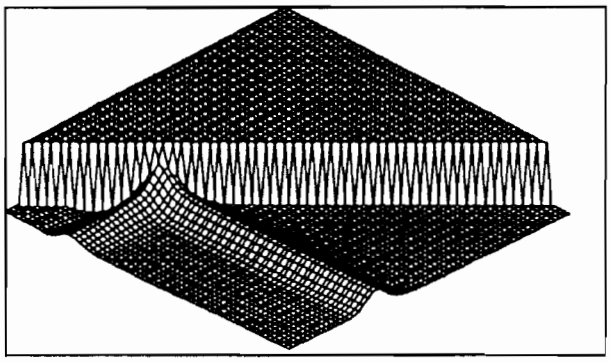

Time = 40s

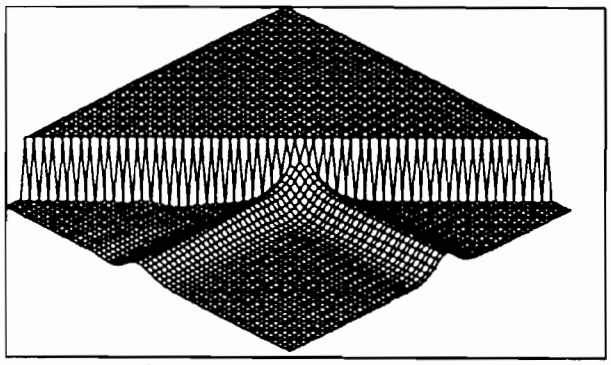

Time = 60s

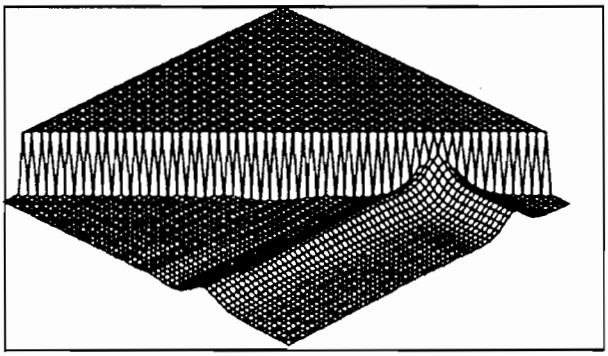

Time = 80s

$\triangle x$ = 14m
$\triangle t$ = 1s
d = 10m
a = 1m

Fig 20 Total reflection of a solitary wave - wall at 45°

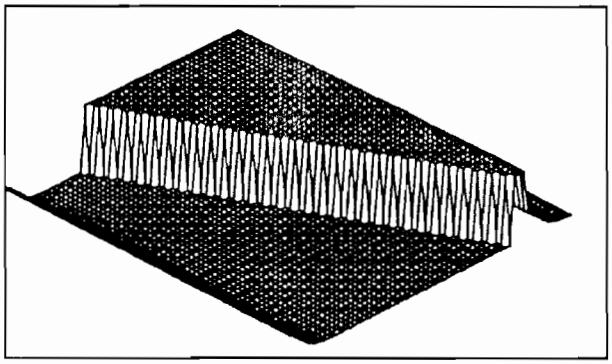

Time = 15s

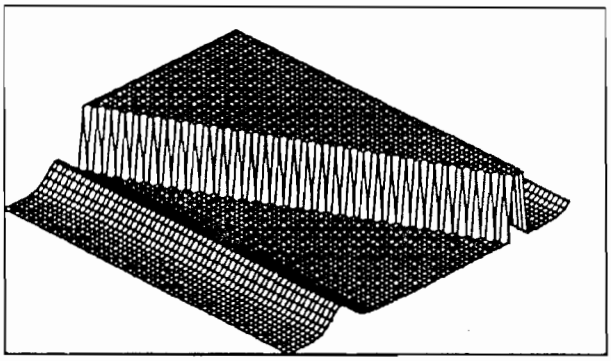

Time = 30s

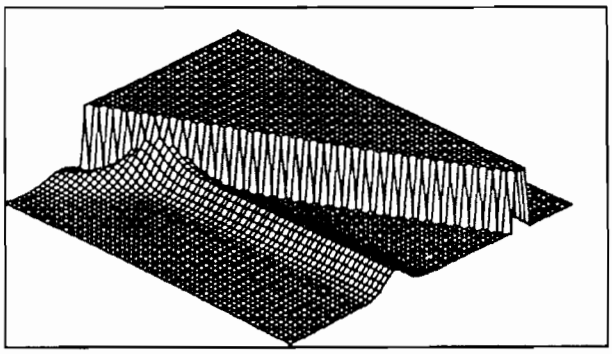

Time = 45s

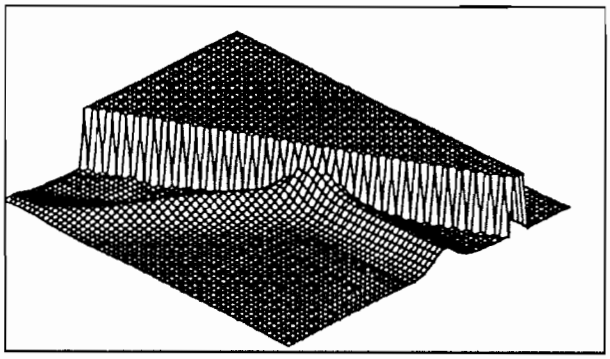

Time = 60s

$\triangle x$ = 14m
$\triangle t$ = 1s
d = 10m
a = 1m

Fig 21 Total reflection of a solitary wave - wall at 60°

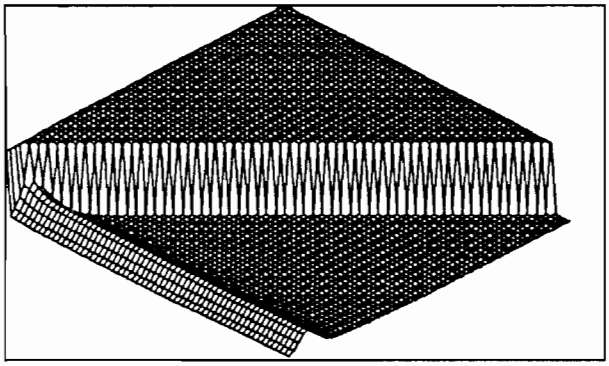

Time = 20s

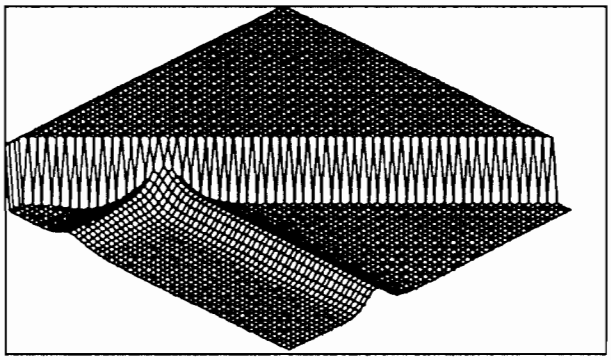

Time = 40s

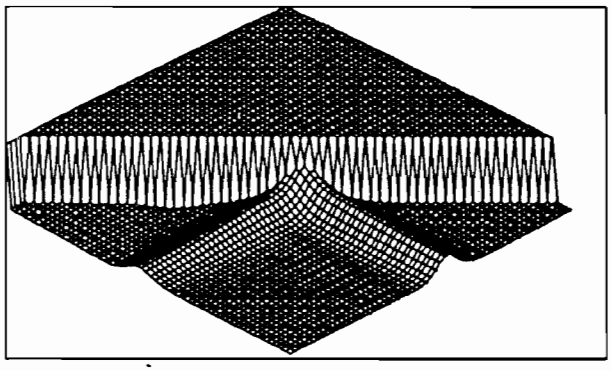

Time = 60s

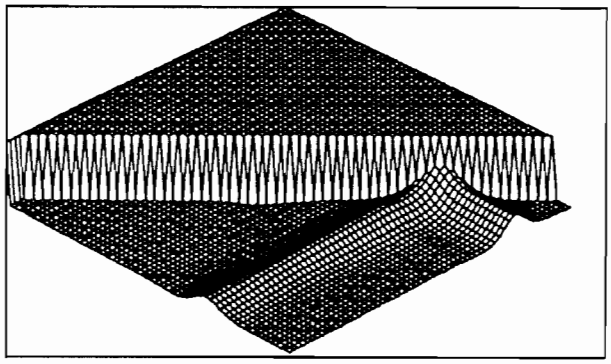

Time = 80s

Δx = 14m
Δt = 1s
d = 10m
a = 1m

Fig 22 Partial reflection of a solitary wave, R = 0.5 - wall at 45°

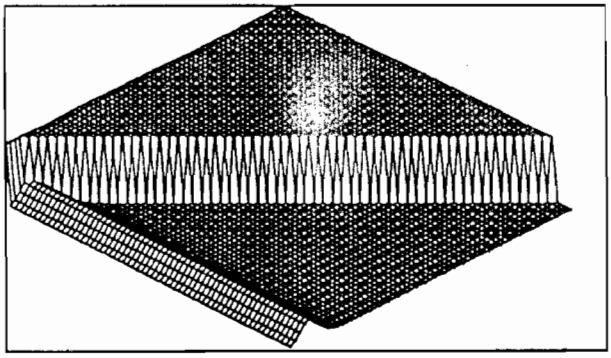

Time = 20s

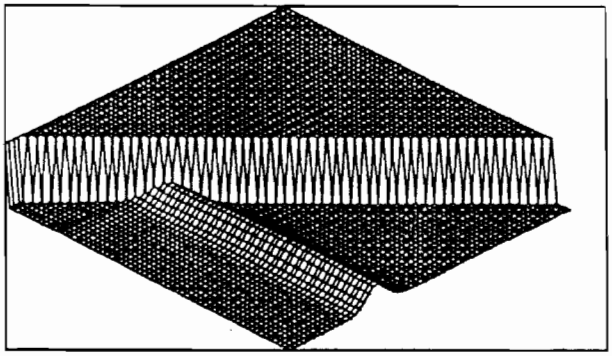

Time = 40s

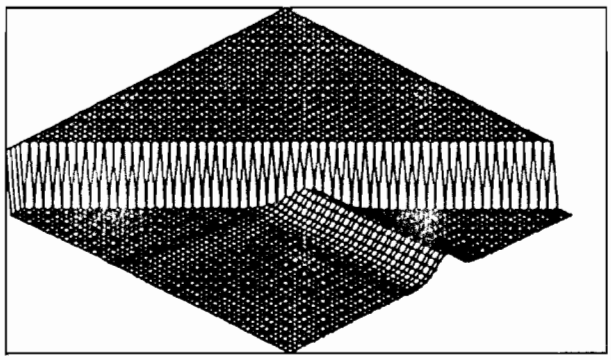

Time = 60s

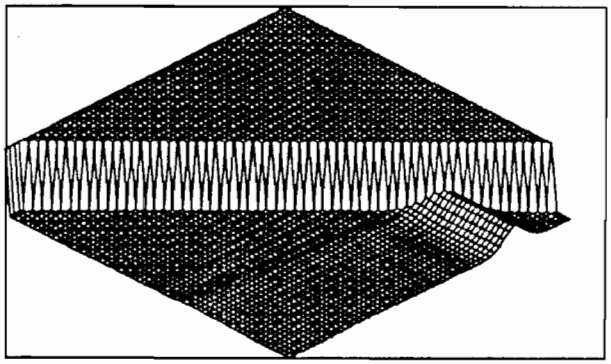

Time = 80s

$\triangle x$ = 14m
$\triangle t$ = 1s
d = 10m
a = 1m

Fig 23 Absorption of a solitary wave - wall at 45°

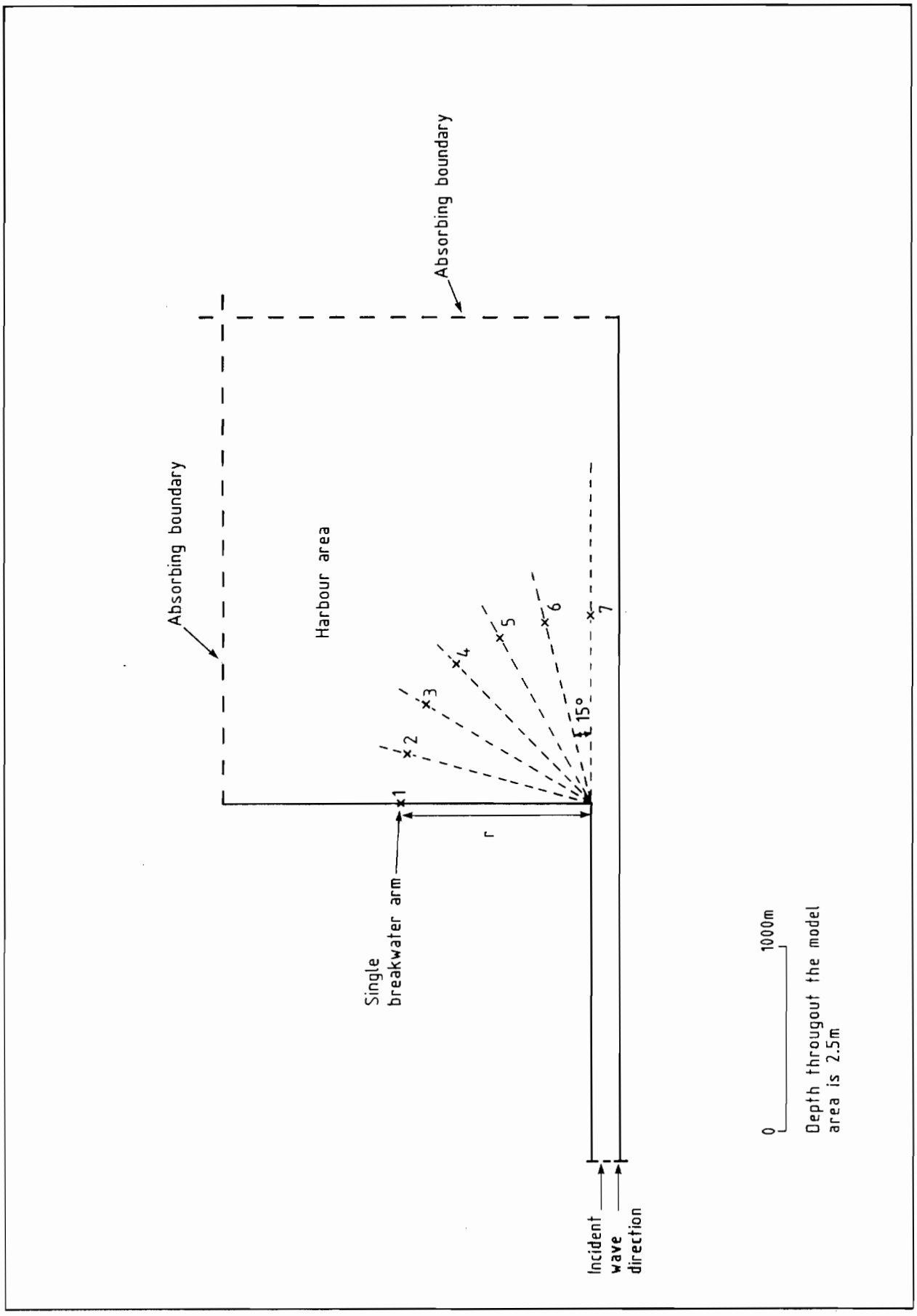

Fig 24 Experimental layout

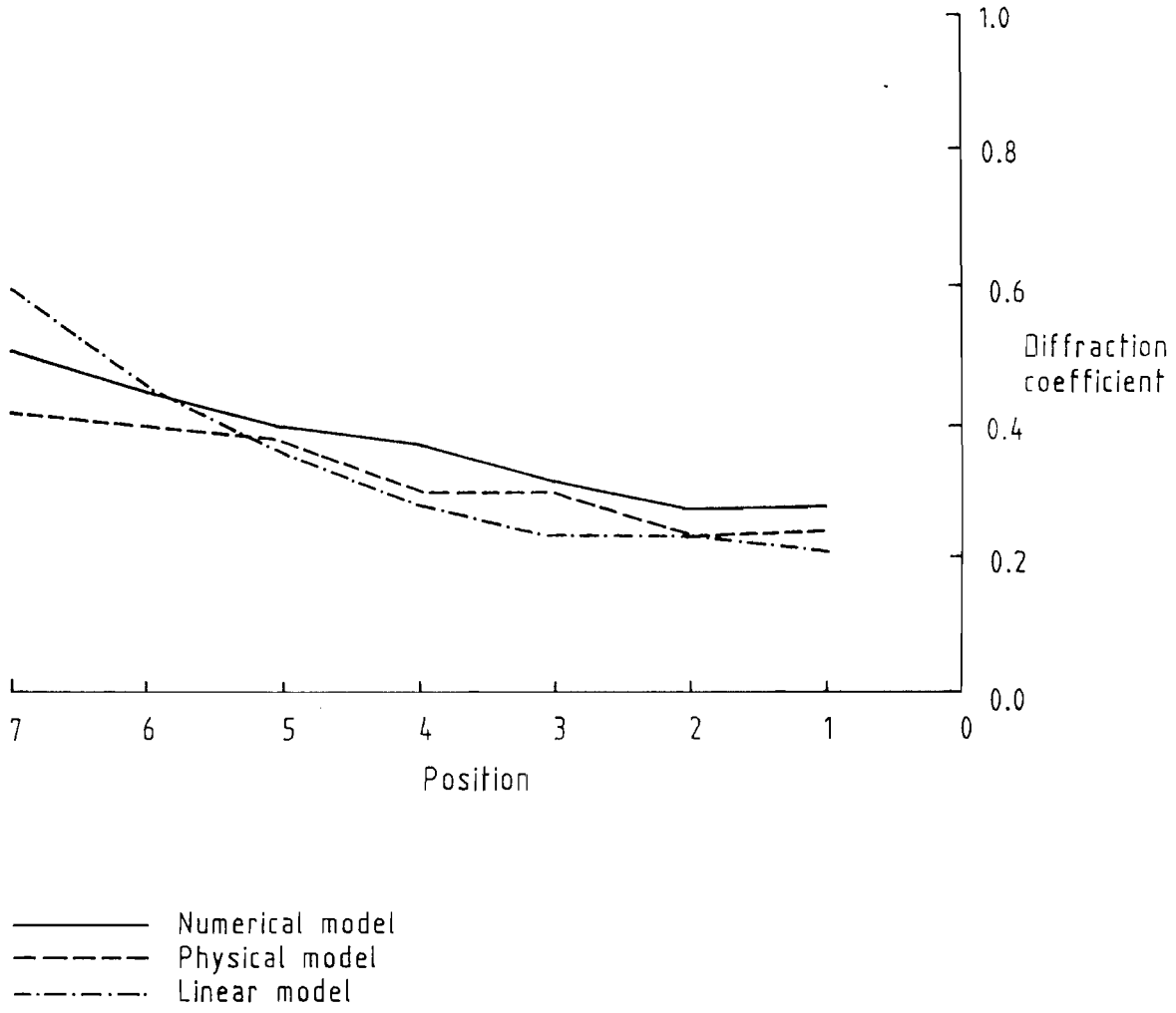

Fig 25 Diffraction coefficients for a primary wave, frequency 0.03Hz, positions at r/L = 1.0 (see Fig 24)

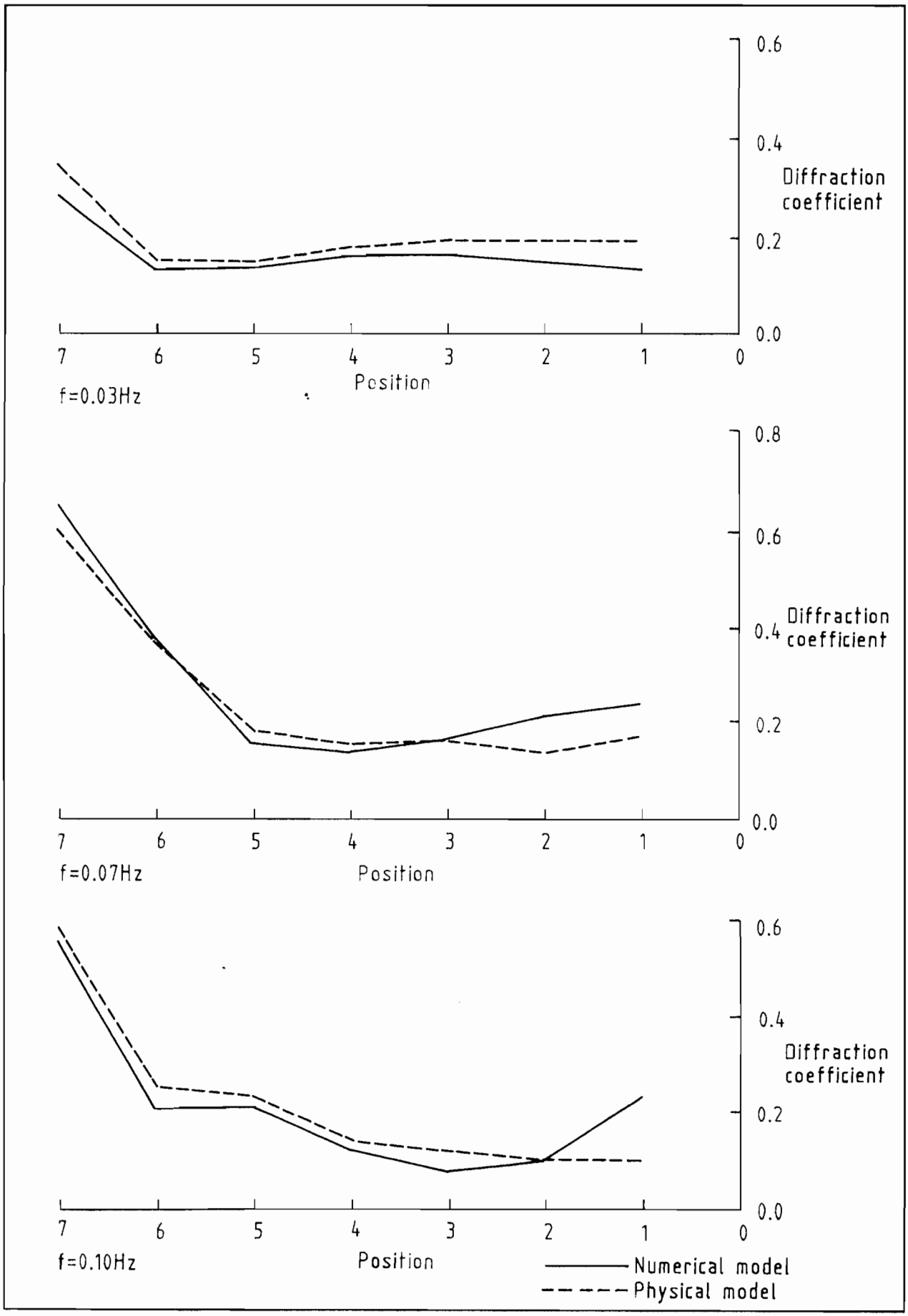

Fig 26 Diffraction coefficients for primary wave groups at positions r/L = 1.0 (see Fig 24)

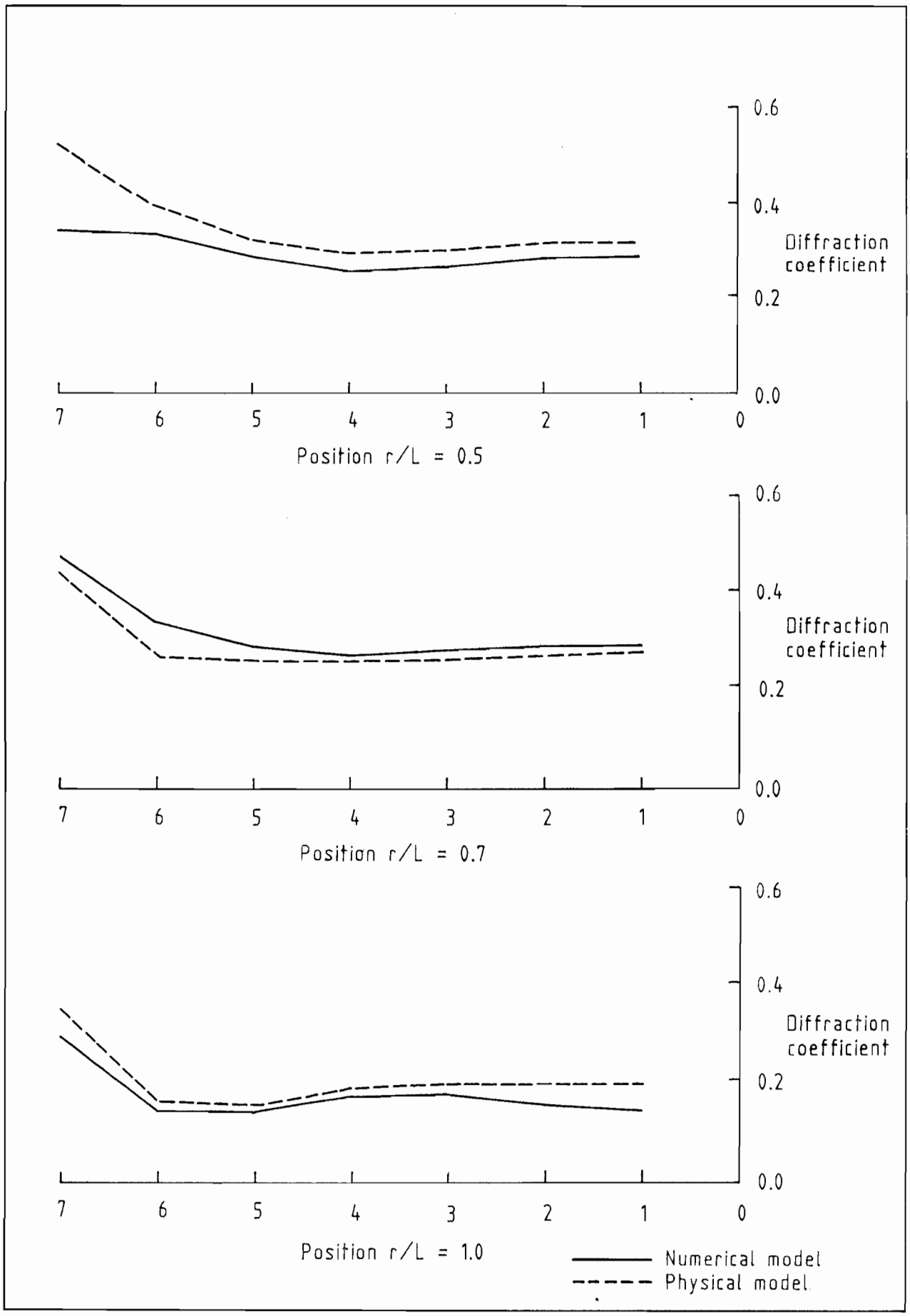

Fig 27 Diffraction coefficients at set down frequency at positions r/L = 0.5, 0.7, 1.0

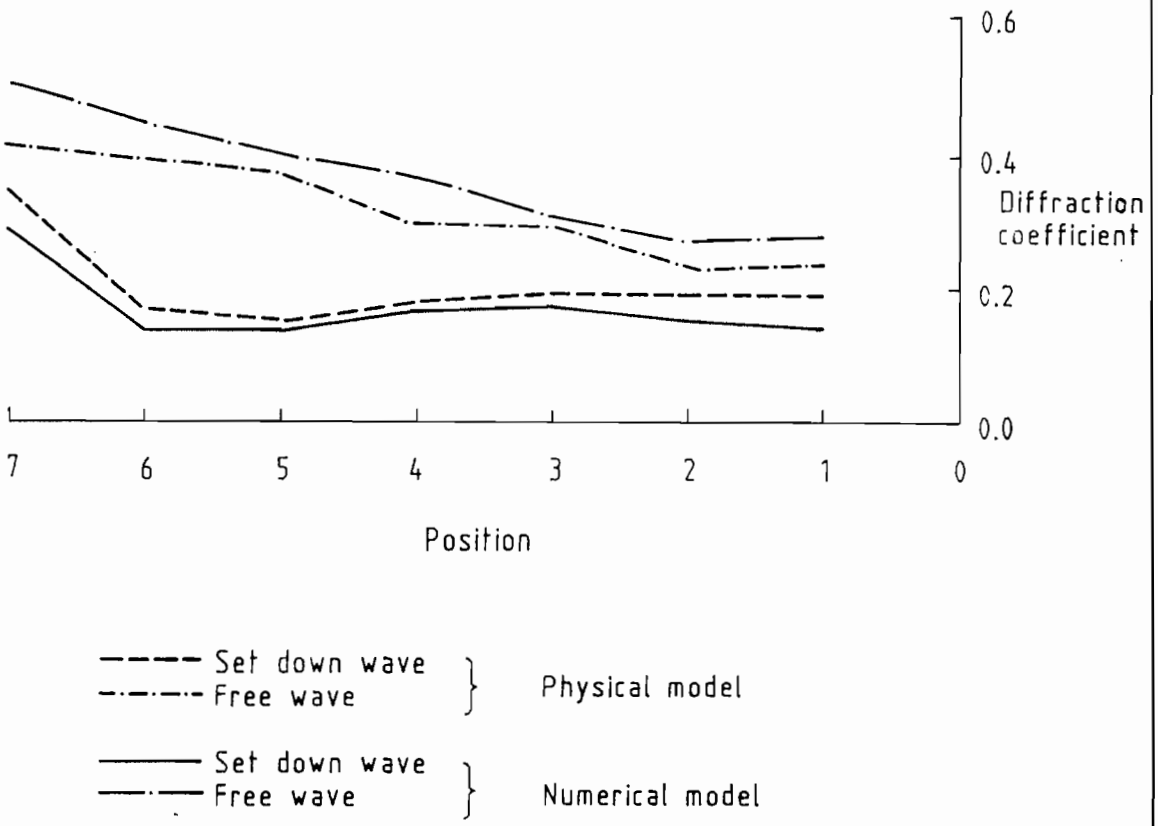

Fig 28 Diffraction coefficients for set down and free waves at 0.03Hz, positions at r/L = 1.0 (see Fig 24)